CHAPTER 9

SOLAR DESALINATION

John H. Lienhard,[1,*] Mohamed A. Antar,[2] Amy Bilton,[1] Julian Blanco,[3] & Guillermo Zaragoza[4]

[1] Center for Clean Water and Clean Energy, Room 3-162, Department of Mechanical Engineering, Massachusetts Institute of Technology, 77 Massachusetts Avenue, Cambridge, Massachusetts 02139-4307, USA

[2] Department of Mechanical Engineering, King Fahd University of Petroleum and Minerals, Dhahran, Saudi Arabia

[3] Plataforma Solar de Almeria, Carretera de Senes s/n, 04200 Tabernas (Almeria), Spain

[4] Visiting Professor of Electrical Engineering, King Saud University, Riyadh, Saudi Arabia

[*] Address all correspondence to John H. Lienhard E-mail: lienhard@mit.edu

In many settings where freshwater resources or water supply infrastructure are inadequate, fossil energy costs may be high whereas solar energy is abundant. Further, in the industrialized world, government policies increasingly emphasize the replacement of fossil energy by renewable, low-carbon energy, and so water scarce regions are considering solar-driven desalination systems as a supplement to existing freshwater supplies. Even in regions where petroleum resources are copious, solar-driven desalination is attractive as a means of conserving fossil fuel resources and limiting the carbon footprint of desalination. Finally, in settings that are remote and 'off-the-grid," a solar driven desalination system may be more economical than alternatives such as trucked-in water or desalination driven by diesel-generated electricity. This article reviews various technologies that couple thermal or electrical solar energy to thermal or membrane based desalination systems. Basic principles of desalination are reviewed. Solar stills and humidification-dehumidification desalination systems are discussed. Membrane distillation technology is reviewed. Current designs for solar coproduction of water and electricity are considered. Finally, photovoltaic driven reverse osmosis and electrodialysis are reviewed. The article concludes by summarizing the prospects for cost efficient solar desalination.

1. INTRODUCTION

Water scarcity is a growing problem for large regions of the world. Scarcity results when the local fresh water demand is similar in size to the local fresh water supply. Figure 1 shows regions of the world in which water withdrawal approaches the difference between evaporation and precipitation, resulting in scarcity.[1−3] The primary drivers of increasing water scarcity are population growth and the higher consumption associated with rising standards of living. A lack of infrastructure for water storage and distribution is also a factor in the developing world. Over time, global climate change is expected to affect existing water resources as well, potentially altering the distribution of wet and arid regions and

ISSN: 1049–0787; ISBN: 1–978–56700–311–6/12/$35.00 + $00.00

NOMENCLATURE

A_{col}	area of solar collector, m^2
A_{mem}	reverse osmosis membrane surface area, m^2
A_{panel}	PV panel area, m^2
C_0	PV panel performance constant, V
C_1	PV panel performance constant, $V\ K^{-1}$
C_{fc}	average concentration of water in the membrane feed channel, mg L^{-1}
C_p	concentration of reverse osmosis permeate water, mg L^{-1}
c_p	specific heat at constant pressure, $J\ kg^{-1}K^{-1}$
E_{net}	annual net electricity delivered to the grid, kWh
FF	membrane fouling factor
F_s	radiation shape factor
G	Gibbs energy of per mole, J mol^{-1}
G_{rad}	solar irradiation, W m^{-2}
GOR	gained output ratio
H	enthalpy per mole, J mol^{-1}
H_{sol}	daily solar incidence on solar collector, J m^{-2}day
h_{fg}	latent heat of vaporization, J kg^{-1}
h	heat transfer coefficient, W $m^{-2}K^{-1}$
h_{fg}	latent heat of evaporation (difference between the enthalpy of saturated vapor and that of saturated liquid at specified temperature), J kg^{-1}
I	PV panel current, A
I_0	reverse saturation current, A
I_{ph}	PV panel light generated current, A
k	thermal conductivity, W $m^{-1}K^{-1}$
K_A	membrane permeability for water, m $bar^{-1}s^{-1}$
K_B	membrane permeability for salt, m s^{-1}
K_{fuel}	annual fuel cost, €
K_{invest}	total investment of the plant, €
$K_{O\&M}$	annual operation and maintenance costs, €
k	Boltzmann constant, J K^{-1}
k_d	real debt interest rate
$k_{insurance}$	annual insurance rate
LEP	liquid entry pressure, bar
L	distance between water surface and glass cover, m
M	molecular weight, g mol^{-1}
$\dot{m}_p$	mass flow rate of purified water, kg s^{-1}
M_d	hourly distillate collected, kg m^{-2}
$\dot{N}$	molar flow rate, mol s^{-1}
n	PV model diode ideality factor (Sec. 7)
n	depreciation period in years (Sec. 6)
Nu	Nusselt number
P	pressure, Pa
pf	polarization factor
ppm	parts per million, mg kg^{-1}
P_w	water partial pressure (at T_w), mm Hg
P_{wg}	water partial pressure (at T_g), mm Hg
$\dot{Q}$	rate of heat transfer into system, J s^{-1}
$\dot{Q}_{least}$	minimum (reversible) rate of heat transfer to separate, J s^{-1}
q	charge of an electron, C
q_b	heat loss through still material to surroundings (ground), W m^{-2}
q_c	convection heat transfer from water to glass cover, W m^{-2}
q_{ga}	heat transfer from the glass cover to ambient air, W m^{-2}
q_e	evaporation heat loss from water to glass cover, W m^{-2}
R_s	PV panel series resistance, Ω
Ra	Rayleigh number
R_{sh}	PV panel shunt resistance, Ω
Re	Reynolds number
S	entropy per mole, J $mol^{-1}K^{-1}$
$\dot{S}_{gen}$	rate of entropy generation in system, J s^{-1} K^{-1}
SW	specific work (per unit mass of purified water), J kg^{-1}
T_{cell}	PV cell temperature, K
T	temperature, K
T_0	system temperature, K
T_H	high temperature from which heat is supplied, K
TCF	water permeability temperature correction factor
U_b	heat transfer coefficient between the basin and surrounding soil, W $m^{-2}K^{-1}$

NOMENCLATURE (Continued)

V	PV panel operating voltage, V
V_p	volume of purified water produced per day, m^3day
$\dot{V}_p$	volume flow rate of purified water, $m^3 s^{-1}$
$\dot{W}$	rate of work transfer into system, J s^{-1}
$\dot{W}_{least}$	minimum (reversible) rate of work to separate, J s^{-1}

Greek Symbols

α	absorptivity
β	angle of inclination of glass cover
μ	dynamic viscosity of air (for Re calculation), kg m^{-1} s^{-1}
ν	kinematic viscosity, m^2 s^{-1}
Δp	pressure difference, Pa
$\Delta \bar{P}$	average pressure applied across the membrane, bar
η_{pump}	isentropic efficiency of pump
η_{pv}	energy conversion efficiency of photovoltaic device
η_{th}	efficiency of solar thermal collector
$\Delta \bar{\pi}$	average osmotic pressure applied across the membrane, bar
ρ	
σ	Stefan Boltzmann constant
τ	transmissivity

Subscripts

a	air (ambient)
b	basin
brine	property of concentrated brine stream
g	glass
least	value in the reversible limit
pure, *p*	property of purified water stream
saline, sw	property of saline feed stream
w	water

Acronyms

AGMD	air gap membrane distillation
CSP	concentrating solar power
CSP+D	concentrating solar power and desalination
DCMD	direct contact membrane distillation
DNI	direct normal irradiance
ED	electrodialysis
LEC	levelized electricity cost
LT-MED	low-temperature multieffect distillation
LT-MED-TVC	low-temperature multieffect distillation powered by thermal vapor compression
LWC	levelized water cost
MD	membrane distillation
MED	multieffect distillation
MENA	Middle East and North Africa
MSF	multistage flash distillation
PT	parabolic trough
PT-CSP	parabolic trough concentrating solar power
PV	photovoltaic
PVED	photovoltaic electrodialysis
PVRO	photovoltaic reverse osmosis
RO	reverse osmosis
SEGS	solar energy generating systems (California, 1984–1991)
SGMD	sweeping gas membrane distillation
TVC	thermal vapor compression
TVC-MED	multieffect distillation powered by thermal vapor compression
VMD	vacuum membrane distillation

raising the salinity of some coastal aquifers. Among these factors, consumption in the developed world can be moderated relatively quickly by government policies aimed at reducing per capita water use, and new supplies can be established through technology; however,

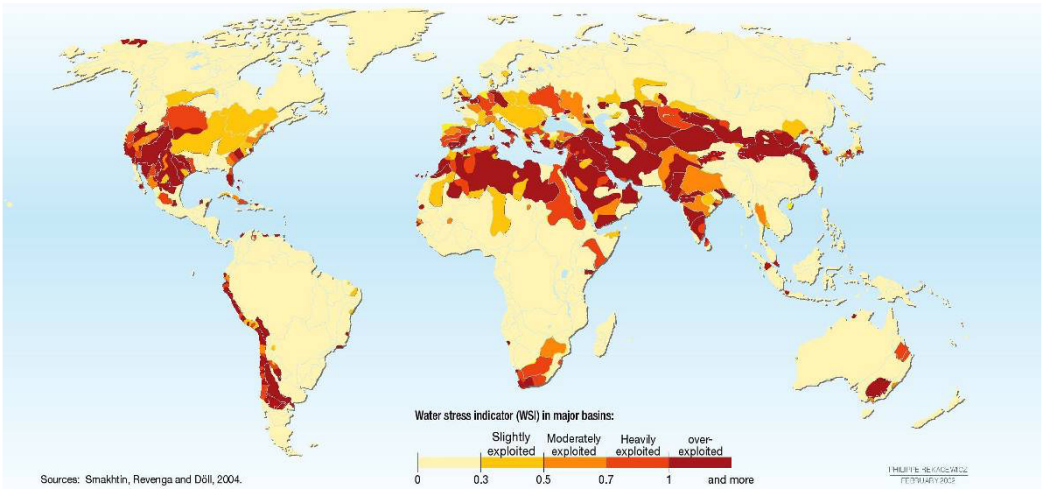

FIG. 1: Regions of water stress, in which total water withdrawals approach the difference between precipitation and evaporation, are show in orange and red.[1]

population growth can be moderated only over very long time scales and infrastructure may not be developed quickly. All of these pressures are moving water-scarce regions toward purification of water supplies that are otherwise too saline for human consumption.

Purification of saline water involves chemical separation processes for removing dissolved ions from water. These processes are more energy intensive than the standard treatment processes for freshwater supplies. In many settings where fresh water resources or water supply infrastructure are inadequate, fossil energy costs may be high whereas solar energy is abundant. Such locations include sub-Saharan Africa and southern India. In the industrialized world, particularly the European Union, government policies increasingly emphasize the replacement of fossil energy by renewable, low-carbon energy, and so water-scarce regions such as Spain or the southwestern United States are considering solar-driven desalination systems as a supplement to existing fresh water supplies. Even in regions where petroleum resources are copious, such as the Arabian or Persian Gulf, solar-driven desalination is attractive as a means of conserving fossil fuel resources and limiting the carbon footprint of desalination. Finally, in settings that are remote and "off-the-grid," a solar-driven desalination system may be more economical than alternatives such as trucked-in water or desalination driven by diesel-generated electricity.

Desalination systems are of two broad types, based upon either thermal distillation or membrane separation.[4,5] In a solar context, the thermal systems will heat saline water and separate the relatively pure vapor for subsequent condensation and use; the engineer's primary challenge is to recover and reuse the heat released in condensation, with minimal temperature difference, so as to make an energy efficient distillation system. Membrane separation systems usually rely on solar-generated electricity either to drive high-pressure pumps that overcome osmotic pressure differentials or to create electric fields that drive electromigration of ions in solution. Solar electricity, in turn, may be produced by either direct solar-electric conversion or by a solar-driven thermal power cycle. Some technologies

will embody both thermal and membrane processes; membrane distillation is an example. All desalination systems, especially those handling seawater or certain wastewaters, must be designed with an awareness of the scale-forming potential of the raw water. Scale formation imposes strong limitations on the thermodynamic performance of thermal desalination systems in particular.

In this chapter, we discuss these issues in the context of various realizations of solar-driven desalination systems. We begin with an overview of basic ideas in the design of desalination systems.

2. BASIC CONCEPTS OF DESALINATION

2.1 Characteristics of Raw Waters

The composition of a raw water source has a guiding effect on the selection of the treatment technology to be used. Different desalination technologies perform most economically in different ranges of salinity, in part because some methods of desalination require greater energy per unit mass as the salinity rises. Further, saline waters may contain a considerable variety of dissolved ions, and the proportions of ions found in low-salinity, or "brackish," ground waters are typically quite different than those in high salinity seawater or those found in wastewaters.

Salinity per se is a term related to the electrical conductivity of the water, and it gives a bulk measurement of the total dissolved solids (TDS, typically in ppm or mg/kg). Well-developed standards define the salinity of seawater through an electrical measurement,[6] and these standards are robust over the various oceans of the Earth.[7] For other waters, a chemical analysis of the raw water is usually needed to determine which ions are present and in what concentration; for example, the ions in ground waters will depend upon the rock formations from which the water is drawn. Table 1 shows the concentrations of ions in representative seawater of 34,500 ppm[8] and in representative brackish ground waters.[9] The ion concentrations of water from a typical fresh surface water supply as distributed to end users are shown for comparison.[10]

In some cases, the concentration of ions is reported by giving the conductivity of water directly, in μS/cm. For distilled water, the conductivity will be roughly 0.5 to 3 μS/cm, and for typical drinking water it will be below 100 μS/cm. Seawater, in contrast, has a conductivity of about 54,000 μS/cm.

Water quality standards fix the maximum allowable concentrations of various contaminants in potable water by considering the health effects of each substance,[11,12] but some ions found in saline water will produce undesirable taste or color at concentrations well below those at which a specific health effect is of concern. In general, a TDS of no more than 500 ppm is recommended in municipal supplies under US EPA secondary regulations,[12] and so a desalination process aims to lower the concentration of all ions in the raw water. Many desalination technologies, particularly distillation technologies, produce very pure water that requires significant post-treatment for compatibility with the distribution system and for palatability.[8] This may typically include pH adjustment, recarbonation to adjust alkalinity, and chlorination.

TABLE 1: Representative ion concentrations for standard seawater, high and low salinity brackish water, and a municipal water supply;[8−10] nr = not reported

Substance (amounts in mg/kg)	**Standard seawater**	**High brackish water**	**Low brackish water**	**Massachusetts water resources authority**
Sodium, Na^+	10,556	1837	90	30
Magnesium, Mg^{2+}	1,262	130	11.7	0.8
Calcium, Ca^{2+}	400	105	96	4.5
Potassium, K^+	380	85	6.5	0.9
Strontium, Sr^+	13	nr	nr	Nr
Chloride, Cl^-	18,980	2970	191	21
Sulfate, SO_4^{2-}	2,649	479	159	8
Bicarbonate, HCO_3^-	140	250	72.6	Nr
Bromide, Br^-	65	nr	nr	0.016
Boric acid, $B(OH)_3$	26	nr	nr	Nr
Fluoride, Fl^-	1	1.4	0.2	1
SiO_2	1	17	24	3.3
Nitrate, NO_3	nr	5.0	nr	0.11
Total dissolved solids	**34,483**	**5881**	**647**	**110**

The thermophysical properties of saline waters are to a first approximation similar to pure water. Extensive data exist for seawater properties.[13−15] Some primary effects of salinity in water are to lower the specific heat capacity (by about 5% for seawater relative to pure water), to raise the density (by about 3.5% for seawater), and to lower the vapor pressure (about 2% lower for seawater, and reasonably well described by Raoult's law). The boiling point is slightly higher and the freezing point is lower for seawater than for freshwater. Each of these is a factor in the precise thermal design of desalination systems. The variation of specific heat capacity with salinity and temperature is shown in Fig. 2.

Additional significant differences between saline water and fresh water stem from the solubility limits of the dissolved ions, including the precipitation of scale-forming salts, such as $CaSO_4$, MgOH, and $CaCO_3$, and the outgassing of CO_2 as the raw water's alkalinity and pH shift during H_2O removal.

2.2 Scale Formation

Scale formation on the heat transfer surfaces of thermal desalination systems normally limits the top temperature of seawater desalination systems to just above 100°C. As explained in Sec. 2.4 below, the low top temperature directly limits the thermodynamic efficiency that can be obtained in thermal desalination. Further, scale formation steers distillation system design away from direct boiling of seawater, since boiling heat transfer surfaces usually operate at temperatures a number of degrees hotter than the local saturation temperature. Instead, distillation systems use liquid films evaporating into a reduced pressure environ-

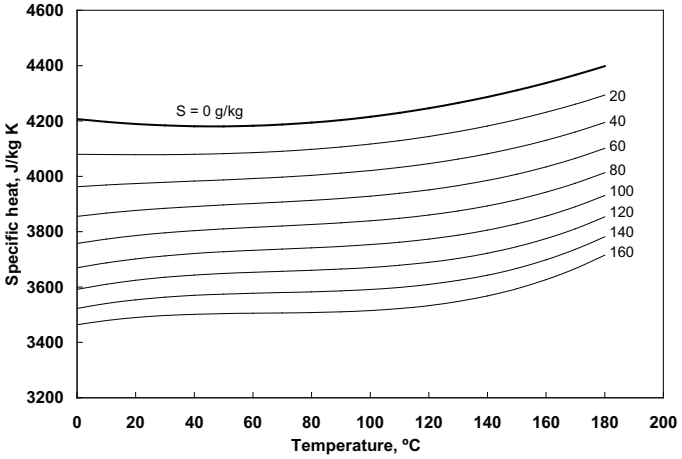

FIG. 2: Seawater specific heat variations with temperature and salinity.[13]

ment or flash evaporation processes. The top temperature range of thermal desalination systems (roughly 60 to 100°C) is well suited to the use of low-pressure steam as a primary heating agent. In large-scale plants, such steam is very often taken from the low-pressure section of an adjacent Rankine or combined cycle power plant. For direct solar thermal desalination, the top temperature limitation reduces the viability of high-temperature optical concentration as a means of raising the feedwater temperature and system thermal efficiency.

The precipitation of scale-forming compounds from saline water is a complex function of temperature, pH, and the degree to which the ions in the raw water have been concentrated by upstream removal of H_2O. Scale formation can be suppressed to some degree by the use of additives, and by process design that confines the most concentrated waters to the lower temperature sections of the system.

For seawater, two relatively insoluble classes of salts are present at near-saturation concentrations. The first class is related to the presence of bicarbonate ion $(HCO_3)^-$ and is called alkaline scale. These scales first appear at about 60°C in the form of $CaCO_3$ (so-called soft scale), becoming dominantly $Mg(OH)_2$ above about 85°C. The second class consists of $CaSO_4$ or its hydrates, which form a hard scale and which appear at temperatures above about 100°C or so, depending upon the amount of water that has been removed from seawater. $CaCO_3$ formation can be suppressed with polyphosphate additives up to 85°C or so. The addition of acids (usually HCl or H_2SO_4) to the seawater provides an inexpensive scale prevention measure up to about 100°C, although with an increased potential for corrosion. Even with careful process control, hard scale cannot be easily suppressed beyond temperatures of 105 to 110°C, and so seawater desalination systems generally will not bring the water to higher temperatures.[5,16,17]

Apart from scale formation in seawater, plant design must also consider biofouling and sludge formation from other material suspended in seawater. The former is especially important in membrane desalination systems. Similar issues can affect brackish ground water desalination systems, depending upon the ions and other material present in the raw

water. Salts such as NaCl, $MgCl_2$, and $CaCl_2$ are orders of magnitude more soluble than the scale-forming salts mentioned here; they become a consideration only after about three-quarters of the water is removed from seawater (as when evaporating seawater to produce sea salt, for example).

2.3 Common Types of Desalination Systems

Desalination of seawater and brackish water has been implemented on a large scale throughout the world. More than 15,000 desalination plants had been installed worldwide by 2010 with a cumulative production capacity of approximately 65 million m^3/day[18] mainly for domestic consumption, with some used in industrial water production. Worldwide water withdrawals for domestic consumption are roughly 1270 million m^3/day,[19] so that cumulative desalination capacity is equivalent in scale to about 5% of worldwide domestic use. In the US, cumulative installed capacity is more than 8 million m^3/day[18] in comparison to publicly supplied water capacity of about 170 million m^3/day.[20] Most of the US capacity uses membrane separation for brackish water desalination. The largest desalination plants, located in the Arabian or Persian Gulf, are thermally driven, seawater desalination plants having capacities of about 1 million m^3/day. The use of desalination has grown dramatically in recent years; in 2001, installed cumulative capacity was less than half that in 2010, only 28.5 million m^3/day.

About 60% of world desalination capacity is based on reverse osmosis (RO),[18] in which saline water is mechanically pressured on one side of a membrane. The membrane has static charge groups on its surface which inhibit the absorption of ion into the membrane; water molecules are soluble in the membrane and diffuse through it from the high-pressure saline side to the low-pressure pure water side. At large scale, these systems are reported to produce water from seawater for as little as \$0.50/m^3. Lower pressure differences, and thus less energy, are required when the saline water has a lower TDS, so RO is significantly less costly for brackish water desalination.

Most of the other desalination plants are based on thermal distillation, either through multistage flash distillation (MSF) or multieffect distillation (MED). The design of these plants is grounded in careful energy recovery in the vapor condensation processes; the recovered heat in turn either drives additional evaporation at a lower pressure or preheats the feedwater. The energy required for thermal distillation is essentially the same irrespective of salinity, so these systems are mainly used for seawater desalination. About 60% of the world's seawater desalination (as opposed to brackish water desalination) is done by thermal methods, mainly MSF, although this fraction is falling steadily as new seawater RO plants are built.[18]

Other, less widely used types of desalination technology include electrodialysis, membrane distillation, and humidification–dehumidification desalination. These are discussed in more detail later in this article.

2.4 Minimum Work of Separation

From the viewpoint of thermodynamics, desalination is a work-driven process that undoes the irreversible mixing of salts into water. This separation process requires the least amount

of work when it can be done reversibly and uses greater amounts of work when the separation process generates entropy through thermal or mechanical irreversibility. A benchmark in the design or assessment of any desalination process is therefore to determine the least, or reversible, work that will be required to remove some percentage of the water from a saline source.

Figure 3 shows a schematic diagram of a desalination system. A saline water stream enters the system, and a purified water stream and a concentrated brine stream leave the system. Work is transferred into the system to effect the separation of salts from the fresh water stream, leaving them in the brine stream. For simplicity, we may consider the inlet and outlet streams to have the same pressure and temperature (this in turn implies that the system exchanges heat with the environment at the system temperature). The first and second laws of thermodynamics applied to this system are

$$\dot{W} + \dot{Q} = (\dot{N}H)_{pure} + (\dot{N}H)_{brine} - (\dot{N}H)_{saline} \tag{2.1a}$$

$$(\dot{N}S)_{pure} + (\dot{N}S)_{brine} = (\dot{N}S)_{saline} + \dot{Q}/T_0 + \dot{S}_{gen} \tag{2.1b}$$

In these equations, $\dot{W}$ is the rate at which work is done on the system, $\dot{Q}$ is the rate at which heat is transferred into the system (which is at temperature T_0), $\dot{N}$ is a molar flow rate, H is the enthalpy of mixture per mole, S is the entropy per mole, and $\dot{S}_{gen}$ is the rate of entropy generation within the system.

These equations may be combined to eliminate the heat transfer rate $\dot{Q}$; with the introduction of the molar Gibbs energy ($G = H - TS$), the work of separation is found in terms of the change in the Gibbs energy of the streams and the irreversibility:

$$\dot{W} = \left[(\dot{N}G)_{pure} + (\dot{N}G)_{brine}\right] - (\dot{N}G)_{saline} + T_0\dot{S}_{gen} \tag{2.2}$$

(We note that similar results may be obtained using the flow exergy rather than the Gibbs energy[14]). It is immediately seen that irreversibility directly raises the work requirements. In the reversible limit, with $\dot{S}_{gen} = 0$, the least work of separation is obtained:

$$\dot{W}_{least} = \left[(\dot{N}G)_{pure} + (\dot{N}G)_{brine}\right] - (\dot{N}G)_{saline} \tag{2.3}$$

The least work will depend upon what fraction of the water is extracted to the pure water stream, and this amount rises steadily as that fraction increases. The least work depends

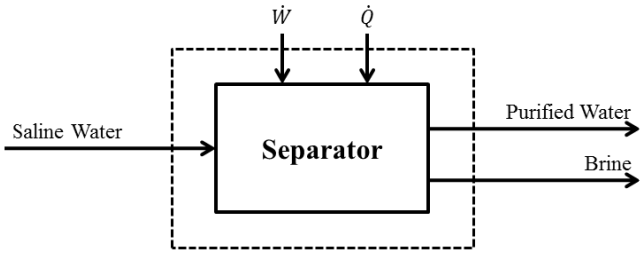

FIG. 3: Schematic diagram of a work-driven desalination system.

more weakly upon the purity of the fresh water stream, with slightly less work required to extract a 500 ppm "pure" stream than a 0 ppm pure stream. Figure 4 illustrates these trends for seawater of varying salinity. As a representative number, at 42% water recovery from seawater with a 0 ppm purified stream, the least work is 3.7 kJ/kg. For a 5000 ppm brackish water, the corresponding least work is about 0.4 kJ/kg.

Thermal desalination may be assessed similarly. In order to do work, heat must be delivered at a temperature T_H above the system temperature T_0. The mechanical work input may be taken to be zero for this purpose (in practice, however, thermal systems require substantial electrical energy for pumping, in addition to the thermal energy requirements). With these two changes, the previous analysis leads to the heat of separation:

$$\dot{Q} = \frac{\left[(\dot{N}G)_{pure} + (\dot{N}G)_{brine}\right] - (\dot{N}G)_{saline} + T_0\dot{S}_{gen}}{1 - T_0/T_H} \tag{2.4}$$

and, in the reversible limit, the least heat of separation

$$\dot{Q}_{least} = \frac{\left[(\dot{N}G)_{pure} + (\dot{N}G)_{brine}\right] - (\dot{N}G)_{saline}}{1 - T_0/T_H} \tag{2.5}$$

In terms of typical numbers, the low temperature will be set by the inlet saline water, perhaps 20°C, and the high temperature will be set by scaling limitations, perhaps 100°C.

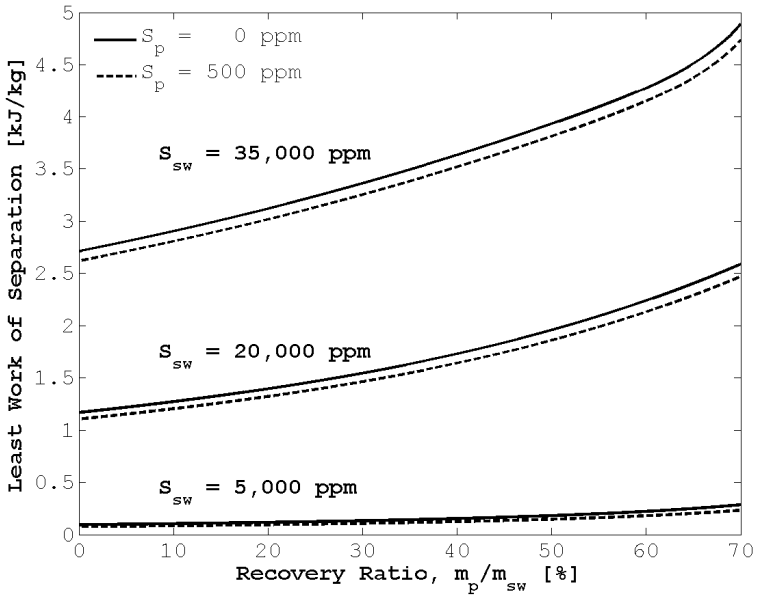

FIG. 4: Least work of separation of water from saline water as a function of water recovery at 25°C. The relative ionic composition of these saline waters is taken to follow that of seawater, even at the lower concentrations. S_{sw} = salinity of saline water; S_p = salinity of purified water; m_p = mass of purified water; m_{sw} = mass of saline feedwater. (Courtesy: K. H. Mistry.)

At 42% water recovery from seawater, the least heat is 17.3 kJ/kg. Obviously, thermal kilojoules are not directly comparable to electrical kilojoules; indeed, the number of thermal kilojoules required to generate an electrical kilojoule depends upon the temperature at which the thermal energy is available and the generation technology applied. Put differently, a kilojoule of low-temperature thermal energy costs only a fraction of a kilojoule of electrical energy. So, the lower energy requirement of a work-driven process relative to a heat-driven process is not meaningful by itself.

The most efficient, large capacity reverse osmosis plants are within a factor of 3 to 4 of the reversible limit. Thermally driven systems are generally within only a factor of 10 or so. The larger difference for thermal systems is to some extent the result of cost-driven design trade-offs. Specifically, a principal irreversibility in thermal distillation processes is entropy produced when heat is transferred through a finite temperature difference in a heater or condenser. Such temperature differences can usually be reduced by employing a larger heat exchanger area, but at the penalty of higher capital cost. As a result, the design value of thermal efficiency may be kept low in order to reduce capital expenditures, thus lowering the overall unit cost of water.

In most thermal desalination systems, the brine and product water may both leave at temperatures above that of the inlet seawater, whereas the least heat calculations above assume equal temperatures. This temperature differential represents a loss of available work and degrades thermal performance.[21]

2.5 Gained Output Ratio and Specific Electrical Work

Several measures of performance have been used for rating the efficiency of desalination systems. Two that will be considered here are the *specific electrical work* (SW) and the *gained output ratio* (GOR).

For electrically (or mechanically) driven systems, the SW is a useful metric. It is the power input to the system, $\dot{W}$, divided by the volume flow rate of purified water, $\dot{V}_p$, typically given in kWh/m^3:

$$\text{SW} = \frac{\dot{W}}{\dot{V}_p} \tag{2.6}$$

For example, the least work of separation for producing pure water from 35,000 ppm seawater at 42% recovery is SW$_{least}$ = 1.03 kWh/m^3. The specific work requirements of typical large-scale reverse osmosis plants range from 3 to 5 kWh/m^3. For mechanical vapor compression desalination systems, SW $\approx$ 7 to 14 kWh/m^3.[22]

For systems driven by thermal energy, it is common to use an energy ratio to compare the rate of heat addition $\dot{Q}$ to the latent heat required to vaporize the mass of purified water produced, $\dot{m}_p h_{fg}$. In the literature, this energy ratio has been referred to as either the performance ratio, PR, or the GOR. We adopt the latter name in the present work:*

$$\text{GOR} = \frac{\dot{m}_p h_{fg}}{\dot{Q}} \tag{2.7}$$

*Both GOR and PR have also been defined in terms of mass flows of the heating steam.[5,23]

A system with a higher GOR distills more water per unit energy. Direct boiling and condensation would produce a GOR of 1 (or less, in view of losses). A fully reversible process would have a GOR of about 120 at a typical MSF top temperature of about 100°C.[24] A typical large multistage flash distillation plant will have a GOR of roughly 6.5 to 9.[25] At a top temperature of about 65°C, which is typical of multieffect distillation, reversible GOR is about 63; existing MED plants have achieved GORs of 9 to 10 without thermovapor compression (TVC),[26] or about 15% of the reversible value; a higher GOR is achievable by using larger heat exchangers and TVC.[27]

From the results previously given, we can relate GOR to entropy generation,

$$\frac{1}{\text{GOR}} = \frac{\left[(\dot{N}G)_{pure} + (\dot{N}G)_{brine}\right] - (\dot{N}G)_{saline} + T_0\dot{S}_{gen}}{(1 - T_0/T_H)(\dot{m}_p h_{fg})} \tag{2.8}$$

which shows that GOR decreases directly with an increase in the entropy generation per unit mass of product, $\dot{S}_{gen}/\dot{m}_p$.

Mistry et al.[21] have provided detailed models for the entropy production and second law efficiency of a wide range of desalination systems. As an example, we may consider a reverse osmosis desalination system operating at 42% water recovery, a feed pressure of 63 barg, and a high-pressure pump efficiency of 86%. The system includes 95% efficient pressure exchangers that use the brine flow to pressurize a corresponding mass flow of the feedwater. The primary sources of entropy generation (per unit mass of product) are the pressure loss as permeate flows through the membranes (at roughly 62 barg of average head loss), the inefficiency of the high-pressure pump, and the inefficiency of the pressure exchanger. The associated entropy production may be shown to be

$$\begin{aligned}\frac{T_0\dot{S}_{gen}}{\dot{m}_p} &= \left[\left(\frac{\Delta p}{\rho}\right)_{memb} + \left(\frac{T_0\Delta\dot{S}_{sep}}{\dot{m}_p}\right)\right] + \left(\frac{\Delta p}{\rho}\right)_{pump}\left(\frac{1}{\eta_{pump}} - 1\right) \\ &\quad + \left(\frac{\Delta p}{\rho}\right)_{pe}(1 - \eta_{pe})\left(\frac{\dot{m}_b + \dot{m}_p}{\dot{m}_p}\right) = \left[\frac{62 \times 10^5}{10^3} - 3920\right] + \frac{63 \times 10^5}{10^3}\left(\frac{1}{0.86} - 1\right) \\ &\quad + \frac{61 \times 10^5}{10^3}(1 - 0.95)\left(\frac{1}{0.42}\right) = 2280 + 1027 + 726 = 4033 \text{ J/kg}\end{aligned} \tag{2.9}$$

The specific work is then

$$\begin{aligned}\text{SW} &= \frac{10^3 \text{ kg/m}^3}{3.6 \text{ MJ/kWh}}\left(\frac{\dot{W}_{least} + T_0\dot{S}_{gen}}{\dot{m}_p}\right) = \frac{10^3 \text{ kg/m}^3}{3.6 \text{ MJ/kWh}}(3690 + 4033) \\ &= 2.15 \text{ kWh/m}^3\end{aligned} \tag{2.10}$$

Hydraulic losses and inefficiencies in the booster pumps will add an additional 10 to 15% to the power requirement of the RO train; in an overall plant estimate, intake and distribution pumping must also be considered. The specific work obtained here is quite similar to that reported for recently built large-scale RO plants.[28,29]

2.6 Performance of Solar Desalination Systems

In contrast to fossil fuel driven desalination, the daily energy supplied to solar desalination systems is cost-free. An increase in energy consumption per unit water produced is reflected as an increase in the required area of solar collectors and thus higher capital cost. Consequently, the performance of solar desalination systems is sometimes stated in terms of the number of liters that may be purified per day per unit area of collector (L/m^2-day). Since the available daily solar energy varies by geographic location and time of year, this figure by itself is not sufficient for performance comparisons. However, we may decompose it to separate the effects of solar incidence and system design.

For an electrically driven system (such as photovoltaic-driven reverse osmosis), we may write the volume of water purified per day V_p per unit area of solar collector A_{col} in terms of the solar energy incidence per day H_{sol}, the specific work of purification SW, and the average daily electrical conversion efficiency of the photovoltaics η_{pv}:

$$\frac{V_p}{A_{col}} = \frac{H_{col}\eta_{pv}}{\text{SW}} \tag{2.11}$$

For a thermally driven system (such as solar-driven humidification–dehumidification), we may write V_p/A_{col} in terms of the solar energy incidence per day H_{sol}, the average daily efficiency of the solar thermal collectors η_{th}, the GOR, and the density of the product water ρ, and latent heat of vaporization of the saline water, h_{fg}:

$$\frac{V_p}{A_{col}} = \frac{H_{col}\eta_{th}\text{GOR}}{\rho h_{fg}} \tag{2.12}$$

These expressions give a first-order separation of the desalination system from the solar energy collection system. The GOR and collector thermal efficiency will depend upon other factors, such as the top and bottom temperatures of the desalination cycle, and these temperatures may vary throughout the day. For both thermal- and electrically driven desalination systems, energy storage may be employed to level the daily cycling and to extend operation into nighttime hours.

3. THE SOLAR STILL

3.1 Introduction

The first man-made large-scale water desalination system, which dates back to the nineteenth century, is the solar still. A solar still is made of an airtight insulated basin that is covered with a tilted glass sheet (Fig. 5). Solar radiation passes through the transparent glass or plastic cover and is absorbed by salty (or brackish) water in the basin so that water is heated and causes evaporation. The water vapor condenses at the inner side of the glazing and the liquid flows by gravity into a trough where it is collected. Basins are painted black to increase solar absorption, and long wavelength radiation cannot pass from the solar still through the glazing. In other words, the greenhouse effect makes the solar still look like a heat trap. A solar still needs flushing to prevent salt precipitation and the flushing frequency depends on the quality of feedwater.

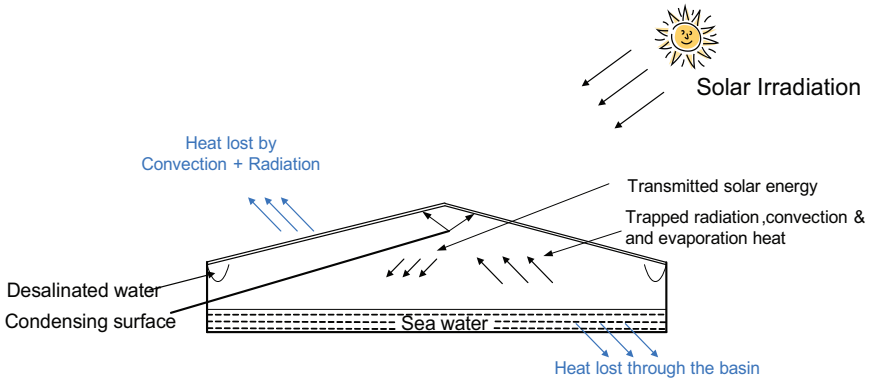

FIG. 5: Solar still.

Solar stills can be classified as passive or active stills. Passive stills will use only the solar energy falling into the unit.[30] In active stills, an external thermal energy source is added to the unit to aid heat addition to the salty or brackish water. Additional heat could be provided by a concentrating solar panel,[31] waste thermal energy,[32,33] or a conventional boiler. Another classification of solar still is based on the geometry: single slope[34] as shown in Fig. 11 (below) or double slope glazing cover[35] as shown in Fig. 5; vertical solar still;[36] conical solar still[37,38] shown in Fig. 6; inverted absorber solar still;[39] and multiple-effect horizontal[40−43] (Fig. 7), or vertical solar stills,[44−48] as shown in Fig. 8. A two-basin still can have a 40–50% increase in productivity, as indicated by Lobo and Araujo.[49] Models of multistage solar collectors[42,48] include an external source of heat, a solar heater, and a vacuum pump to enhance evaporation rate as depicted in Fig. 7. The modeling of a multistage solar still follows simple heat and mass balances.[42,48] However, due to space limitations, only the basic case of a single-stage solar still will be discussed in detail here.

Other attempts to increase the solar still productivity include increasing the heat and mass transfer surface area through methods such as using: sponge cubes;[50] wicks[51] as shown in Fig. 9; charcoal,[52,53] which is reported to increase productivity by 15%; or violet dye in the water,[54] which resulted in a 27% increase in productivity due to higher solar absorptivity.

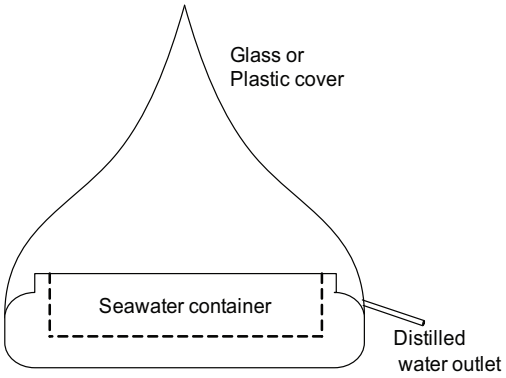

FIG. 6: Water-cone solar still.

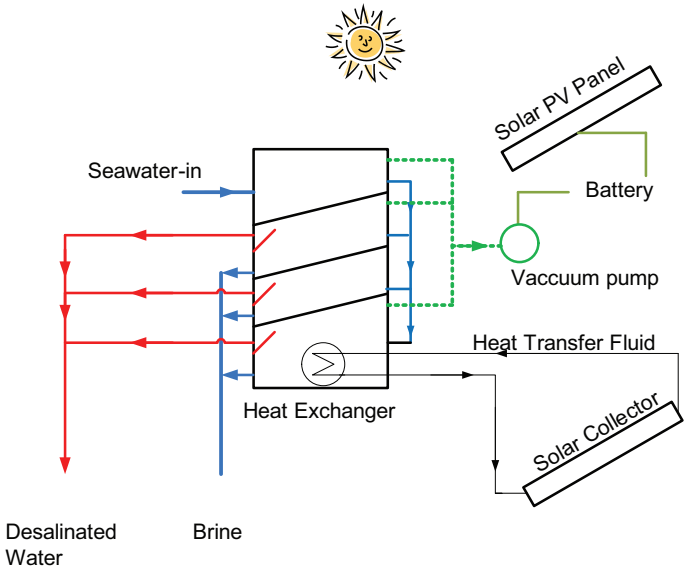

FIG. 7: Multistage solar collector under vacuum.

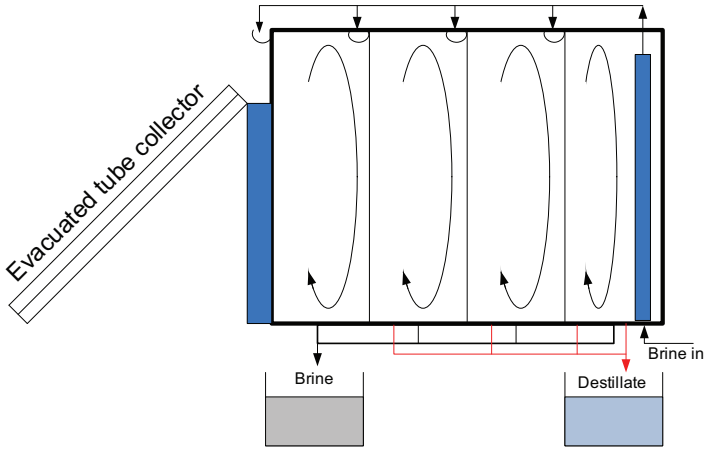

FIG. 8: Multieffect vertical solar still with a solar heater.

Furthermore, adding energy storage units to the solar still leads to a significant increase in productivity.[55] Thermodynamic and economic considerations in solar stills are given,[56] whereas Abdel-Rehim and Lasheen[57] proposed a solar still that includes a heat exchanger. Oil, heated by solar energy, circulates from a solar collector to a heat exchanger placed in the still in order to heat the saline water for higher productivity. Increasing the solar radiation into the still was also reported through the use of a reflecting surface (Fig. 10).

Solar still designs in which the evaporation and condensing zones are separated are described by Refs. 58 and 59. In addition, a device that uses a “capillary film distiller” was implemented by Bouchekima et al.[60] and a solar still integrated in a greenhouse roof is

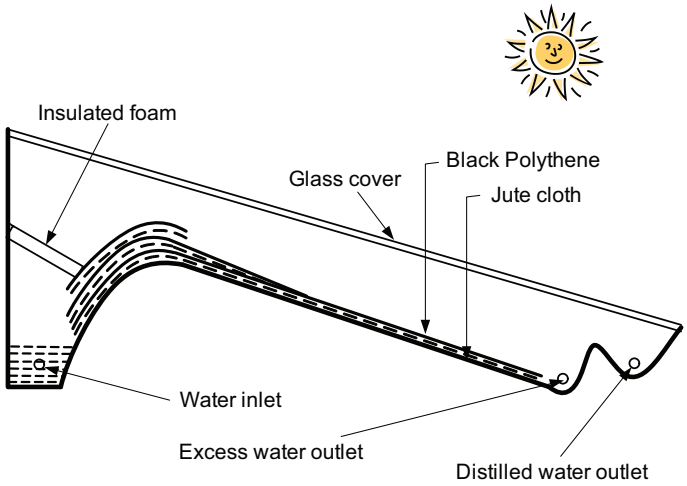

FIG. 9: Inclined solar still with multiple wicks.

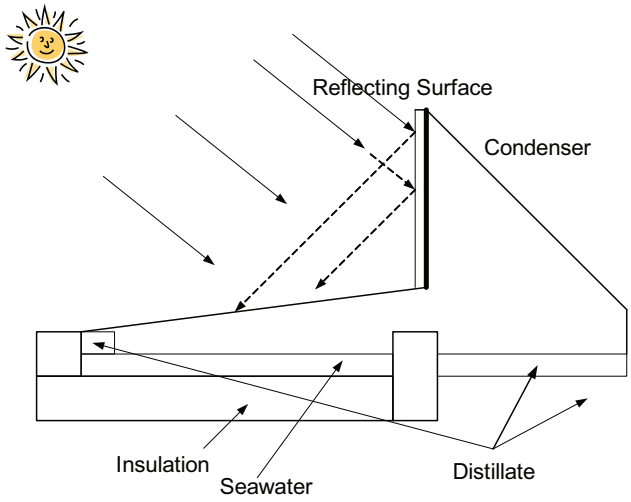

FIG. 10: Solar still with a reflecting surface and a separate condenser.

reported.[61−63] Another class of active solar stills raises the distillation temperature using flat-plate collectors connected to the stills.[64,65]

The distance of the gap between the evaporator tray and the condensing glass (or plastic) surface has a considerable influence on the performance of a solar still, which increases with decreasing gap distance. Cascaded-type solar stills[66] have been developed in which shallow pools of water are arranged in cascade, covered by a sloping transparent enclosure. The evaporator tray is usually made of a piece of corrugated aluminum sheet painted flat black.

Sharma and Mullick[67,68] developed a semiempirical equation to estimate glass cover temperatures to calculate the upward heat flux and evaporation. They calculated the changes in the heat transfer coefficients over a complete day.

Factors influencing the still productivity were investigated by Cooper,[69] who indicated the upper limit of solar still productivity both theoretically and experimentally. Mimaki et al.[70] carried out measurements of performance parameters of both basin-type and tilted wick solar stills and compared the measured values with a theoretical analysis of heat and mass transfer processes indicating the superiority of the tilted wick still.

Yadav and Prasad[71] investigated analytically the transient behavior of a basin-type solar still and pointed out the effect of energy storage for continuous distillate production. Yadav and Yadav[72] have also considered a solar still integrated with a tubular solar energy collector and performed a transient analysis for the still performance.

Recently, Phadatare and Verma[73] showed the superiority of using a glass cover for a plastic solar still in comparison with a Plexiglas cover in terms of heat transfer coefficients as well as water evaporation and distillate productivity. Khalifah and Hamood[74] investigated experimentally the correlations that were used to show how the productivity is affected by brine depth, using a violet dye.

Antar and Zubair[34] studied the effect of property variation in the still performance. They used more reliable and updated correlations to predict the heat transfer coefficients, considering the effect of buoyancy that is attributable to the fact that water vapor reduces the gas mixture density relative to air alone. Table 2 lists the productivity of various designs of solar stills reported in the literature.

3.2 Modeling Solar Stills

Typical design problems encountered with solar stills relate to brine depth, vapor tightness of the enclosure, distillate leakage, methods of thermal insulation, and cover slope, shape, and material.

3.2.1 Mathematical Formulation

Energy balance for the solar still is shown schematically in Fig. 11. Various heat transfer components are shown in this figure, including solar irradiation falling on the solar still, heat transfer within the solar still that includes the thermal radiation transmitted through the glass cover to the water surface and heat transfer by convection, radiation, and evaporation from the water surface back to the glass cover, heat loss through the still opaque material, and heat loss to the ambient air through both convection and radiation heat transfer modes. It is assumed that the capacitance of the glazing is small compared to that of water and basin and hence it is neglected in the present work. The transient energy balance equations for the solar still as described by Duffie and Beckman,[77] based on the original analysis of Dunkle,[78] are summarized in this section.

Considering the thermal capacitance of saline water, the energy balance is

$$\alpha_w \tau\, G = q_{ga} + q_b + m\, c_P \frac{dT_w}{dt} \tag{3.1}$$

where energy losses from the water body to the glass cover and from the water body to the base of the still can be written, respectively, as

TABLE 2: Various values of still yield reported in the literature

Reference	Geometry	Production, L/m^2-day	Other details
Ismail[38]	Hemispherical	2.8–5.7	
Cappelletti[75]	Conventional	2/5 (winter/ summer)	
Al-Hinai et al.[76]	Double slope	4 (annual average)	
Al-Hinai et al.[44]	Single effect Double effect	4.15 6.1	
Jubran et al.[48]	Multistage solar still with expansion nozzle, recovery features, and a vacuum pump	9	3 stages
Nijmeh et al.[54]	Using violet dye/charcoal	5.3	17% improvement after adding the dye/charcoal
Abdel Rahim and Lasheen[57]	External solar heater (using a heat transfer fluid)	2, 2.75 (conventional/ modified)	The modification is by adding a heat transfer fluid in a separate circuit to heat water in the basin
Ahmed et al.[42]	Multistage still with an effective vacuum pump	18 (for P = 0.2 bar) 10 (for P = 1.0 bar)	Yield decreases with the water height in the basin

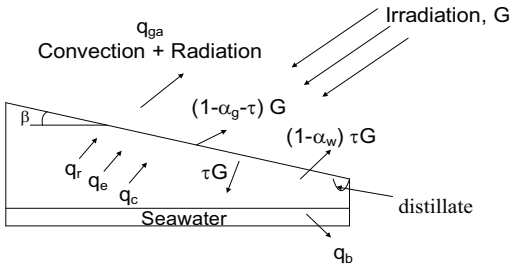

FIG. 11: Single-slope solar still.

$$q_{ga} = q_r + q_c + q_e \tag{3.2}$$

$$q_b = U_b\,(T_w - T_b) \tag{3.3}$$

Heat flux from the water to the cover by radiation Q_r can be estimated using the relation

$$q_r = F_s \sigma (T_w^4 - T_s^4) \tag{3.4}$$

In this expression, F_s is the radiation shape factor. It depends on the geometry of the still and the nature of solar radiation. The geometry can be approximated by two parallel

planes. The radiation involved is considered as diffuse radiation in long wavelengths, so that specular reflection between the transparent cover and water surface is negligible. As a result, the shape factor can be closely approximated by the emissivity of the water surface, usually taken as 0.9 for the conditions inside the still. Thus, Eq. (3.4) can be approximated as

$$q_r = 0.9\sigma(T_w^4 - T_s^4) \tag{3.5}$$

The heat flux from the water to the cover by natural convection and evaporation can be written, respectively, as

$$q_c = h_c(T_w - T_g) = h_c \Delta T \tag{3.6}$$

$$q_e = m_d h_{fg} \tag{3.7}$$

The heat loss from the transparent cover to the surroundings depends both on radiation to the sky and convection loss coefficient due to the surrounding (ambient) air. Radiation to the sky depends on the effective sky temperature, which is sometimes taken as 11°C less than the ambient temperature. The convective portion is a function of the wind speed. This heat transfer component (losses) can be expressed as

$$q_{ga} = \varepsilon_g \sigma[T_g^4 - (T_a - 11)^4] + h_{ga}(T_g - T_a) \tag{3.8}$$

Equations (3.1) to (3.8) represent the key equations for solar still analysis. In addition, the convection correlations that describe convection from the water surface to the glass cover as well as from the glass cover to the environment are described below.

3.2.2 Natural Convection within the Solar Still

Improvements to natural convection correlations within the still have been provided by many researchers based on either experiments[79,80] or detailed analysis that considered the tilt angle of the glass cover.[81] This correlation was modified by Antar and Zubair[34] for solar still applications by replacing the temperature difference with an equivalent temperature difference, taking into account the added buoyancy attributable to the fact that water vapor is lighter than air. Therefore, the modified heat transfer coefficient can be expressed as

$$\mathrm{Nu} = \frac{h_c L}{k_{fluid}} = 1 + 1.44\left[1 - \frac{1708\,(\sin\,1.8\,\beta\,)^{1.6}}{\mathrm{Ra}\,\cos\,\beta}\right]\left[1 - \frac{1708}{\mathrm{Ra}\,\cos\,\beta}\right]^{+} + \left[\left(\frac{\mathrm{Ra}\,\cos\,\beta}{5830}\right)^{1/3} - 1\right]^{+} \tag{3.9}$$

where the meaning of the plus sign (+) in the exponentiation is that if the term is negative (< 0), it is taken = 0 (only positive values are considered); β is the angle of inclination of the cover, and Ra is the Rayleigh number.

Following the approach suggested by Dunkle,[48] the modified temperature difference is used in the Raleigh number equation. This can be written as

$$\Delta T' = (T_w - T_g)\left[\left(\frac{P_w - P_{wg}}{P_{ambient}\,(M_{dry\,air}/[M_{dry\,air} - M_{w\,vapor}]) - P_w}\right)(T_w + 273)\right] \quad (3.10)$$

By the analogy between heat and mass transfer, the distillate mass flow rate (productivity) can be written as

$$m_D = 9.15 \times 10^{-7} h_c\,(P_w - P_{wg}) \quad (3.11)$$

3.2.3 Wind Loss Coefficient

There are many convection heat loss coefficient relations available in the literature dealing with the glass cover to ambient air; however, the formula given by Sparrow et al.[82] and recommended by Duffie and Beckman[77] appears to be the most reliable for predicting heat loss from the glass cover. It is given by

$$\mathrm{Nu} = \frac{h_{ga} l}{k_{air}} = 0.86\ \mathrm{Re}^{1/2}\mathrm{Pr}^{1/3} \quad (3.12)$$

This equation is based on experiments on rectangular plates at various orientations and was found to give reliable predictions for the Reynolds number range of 2×10^4 to 9×10^4, where the characteristics length l is defined as 4 times the plate area divided by the still perimeter.

Note that the solution of the above coupled (heat and mass transfer) equations is very sensitive to thermophysical properties. The present solution procedure was based on variable properties (c_P, μ, α, ρ, k, h_{fg}, P_w, P_g, etc.), which were updated when any value of the temperature is calculated.

3.3 Solar Still Performance

The productivity of the solar still follows the solar irradiation profile. It increases until midday and then decreases until sunset, as shown in Fig. 12. The figure also shows the

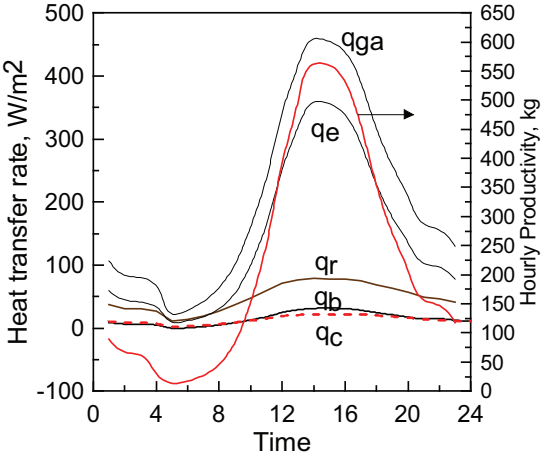

FIG. 12: Solar still performance, heat transfer rates, and productivity.

calculated magnitude of each heat transfer component. The results show that both higher solar intensity and effective glazing cooling (through high convection loss from the glazing to the atmosphere) increase the solar still productivity. If the still is well insulated, the stored heat maintains evaporation after sunset. The gained output ratio is expressed in terms of instantaneous as well as overall efficiency by Balan et al.[30] and Tiwari and Singh.[83] The instantaneous efficiency is given in Eq. (2.7), where instantaneous values are used in the equation, whereas the overall efficiency represents these variables integrated over a defined period of time (in the case of active solar stills, the denominator is extended to include the energy provided by the external heat source).

The gained output ratio of a solar still is typically low (GOR$\sim$0.5). This performance parameter depends on various operating parameters which were evaluated in detail by Antar and Zubair.[34] Solar irradiation, wind speed, depth of saline water, and ambient temperature are among the major parameters that influence the solar still productivity.

3.4 Summary Comments on Solar Stills

From the work of a number of previous researchers, it has been shown that the performance of the solar still is affected by many design and operating parameters. In order to improve the performance of a solar still various steps can be taken, including: increasing the energy input (either naturally from solar radiation in summer versus winter, or through the use of reflecting mirrors or external heat sources as in active stills); increasing the evaporative surface area (through the use of wicks, or sponge cubes of charcoal); lower condensing surface temperature (by separating it from the heat absorbing basin); or introducing heat recovery (as in multistage and multieffect stills). In addition, low ambient temperature and lower depth of saline water are among the factors that increase the distilled water production of the solar still.

4. HUMIDIFICATION–DEHUMIDIFICATION DESALINATION

4.1 Introduction

Solar stills generally integrate the functions of solar collection, water heating, evaporation, and condensation into a single volume. This configuration results in considerable thermal inefficiency. For example, the warm brine can exchange heat directly with the condenser surface (the glazing) by natural convection and infrared radiation. As a result, solar stills normally have a low GOR and require relatively large areas in order to produce fresh water.

Humidification–dehumidification (HDH) desalination uses separate components for each of the thermal processes, allowing each component to be independently designed and allowing much greater flexibility in the design of the thermodynamic cycle for vaporizing water into air and subsequently condensing the vapor.[84] The advantage of HDH over a solar still is a significantly higher GOR, resulting in a smaller total area of solar collector for a given water demand. More broadly, HDH systems are regarded as having an advantage over some other technologies, such as reverse osmosis, in that they involve relatively simple, inexpensive components and can operate over a wide range of raw water quality without the need for complex maintenance operations. This makes HDH more suitable for

deployment in the developing world, where capital investment and technical support may be limited.

The basic drawback of the HDH system is that the thermal energy requirements are still relatively high in comparison to other technologies.

4.2 Classification

HDH cycles may be classified according to whether air or water is heated and according to whether the air or water circuit is open or closed loop. A water-heated, open-air closed-water cycle is shown in Fig. 13. Air-heated cycles with open-loop water and air, closed-air and open-water loops, and closed-water with open-air loops are shown in Figs. 14–16, respectively.

Studies of water-heated cycles are reported by Al-Hallaj et al.,[85] Muller-Holst et al.,[86] Al-Hallaj and Selman,[87] Dai et al.,[88] Orfi et al.,[89] and Shaobo et al.,[90] among many others.

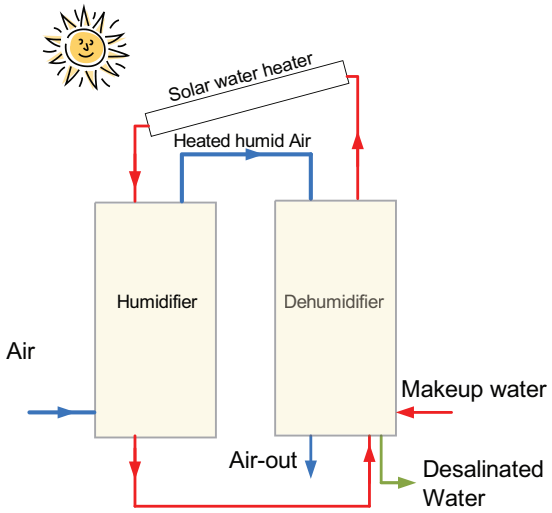

FIG. 13: Water-heated system with open-air and closed-water loops.

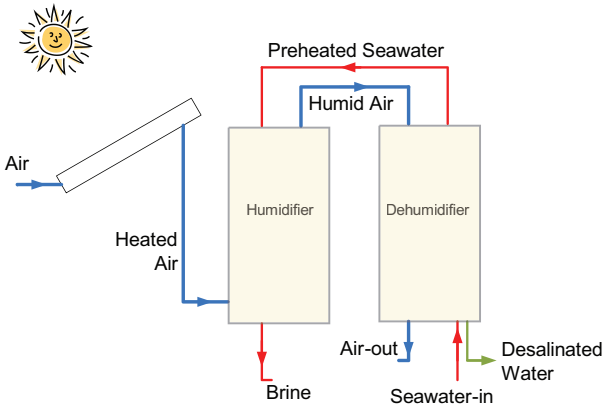

FIG. 14: Air-heated cycle with both air and water streams open.

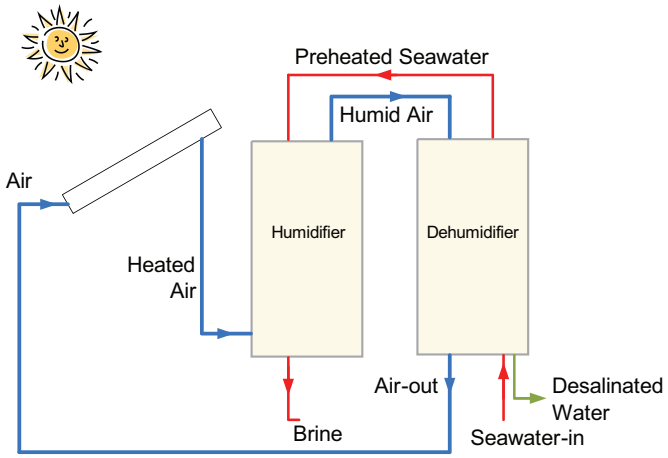

FIG. 15: Air-heated cycle with closed-air loop.

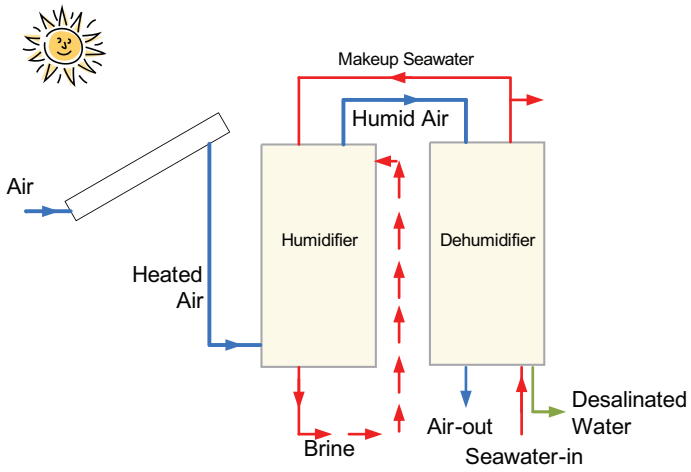

FIG. 16: Air-heated cycle with closed-water loop.

Air heating has been investigated by Chafik et al.,[91–93] Fath and Ghazy,[94] and Yamali and Solmus.[95,96] Chafiq[93] proposed a low-cost solar collector based on polymeric materials. However, this collector had low efficiency compared to commercial units.

Nafey et al.[97] used dual solar heaters to heat both air and water separately in an HDH system. A different configuration was used by Xiong et al.,[98,99] where a steam generator and water heating tank in an HDH system with only one baffled shell and tube column was used in place of separate humidifier and dehumidifier units. Yanniotis and Xerodimas[100] considered two types of air humidifiers as a part of the multistage solar desalination process. The first one was a tubular spray humidifier and the second one was a pad humidifier. They also presented some computational results for the pad humidifier. Their results showed no substantial differences between both types in terms of pressure drop. The evaporation rate was higher for a thicker pad system at high air-to-water flow rate ratios. Fath

and Ghazy[94] reported that air-heated HDH system productivity improved with increased solar energy for air heating, decreased wind velocity, and increased air loop flow rate up to a certain value. They also reported that the dehumidifier size has an insignificant effect on the performance. The latter is an issue of controversy among investigators that requires further exploration. Table 3 lists some HDH systems in the open literature along with their reported production rates.

4.3 Analysis

Thermodynamic analysis of these cycles is generally based on the mass and energy balances for each component in the cycle. We now discuss some of the energy balance equations that can be combined to form a whole cycle balance for any of the aforementioned cycles. The main components of a cycle are the solar collector, the humidifier, and the dehumidifier. Additional components may be added such as pumps and water tanks.

TABLE 3: Some HDH systems reported in the literature

Comments	Production	Heating mode	Reference
Solar area 6 m^2. No energy recovery	3 L/m^2-day (GOR < 0.5)	Water heating	Ben Basha et al.[101]
Forced circulation of air, multipass shell and tube condenser, and wooden shaving packing in the humidifier	12 L/m^2-day (GOR < 4)	Water heating	Farid et al.[102]
Thermal storage, natural air draft, 38 m^2 collector area	13 L/m^2-day (GOR = 3 – 4.5)	Water heating	Muller-Holst et al.[86]
Packed-bed humidifier, air-cooled dehumidifier	9 L/day	Water and air heating	Nafey et al.[103]
2 m^2 solar collector area, humidifier and condenser specific areas are 14 and 8 m^2/m^3	8 L/m^2-day (GOR < 2)	Water heating	El-Hallaj et al.[85]
Natural and forced air flow, heat recovery in the condenser	Up to 5 kg/h (GOR < 4)	Air heating	Nawayseh et al.[104]
5 heating-humidification stages. Forced air circulation. Total collectors area ~ 127 m^2.	4 L/m^2-day (total 516 L/day)	Air heating	Houcine et al.[105]
Single-stage, double-pass solar collector, pad humidifier and finned tube dehumidifier and 0.5 m^3 water storage tank. No heat recovery. Water may be heated in the storage tank to increase production significantly.	4 kg/m^2-day (increased to 10 kg/m^2-day upon operating the water heater)	Air heating (in addition to an evacuated tubular solar water heater)	Yamali and Solmus[95,96]

4.3.1 Solar Collector Energy Balances

Glazing

$$\dot{m}_g c_{p,g} \frac{dT_g}{dt} = I\alpha_g A_c + q_{r,p-g} - q_{c,g-amb} - q_{r,g-sky} - q_{c,g-f} \tag{4.1}$$

Air pass

$$\dot{m}_f c_{p,f} \frac{dT_f}{dt} = q_{c_{p,f}} + q_{c_{g-f}} - \dot{m}_f c_{p,f}(T_{f,out} - T_{f,in}) \tag{4.2}$$

Absorber plate

$$m_p c_{p,p} \frac{dT_p}{dt} = I\alpha_p \tau_g A_c - q_{c_{c,p-f}} - q_{loss} - q_{r,p-g} \tag{4.3}$$

Note that $\dot{m}_f$ is the mass flow rate of the fluid passing through the solar collector (air or water), c_p is the specific heat capacity, T is the temperature, t is time, q is the heat transfer rate, α is the surface absorptivity, τ is the transmissivity, and the subscripts r, c, g, f, p represent radiation, convection, glass, feed, and absorption plate, respectively, whereas A_c is the surface area of the collector. In addition, the term Q_{loss} refers to the heat loss from the absorption plate to the surroundings through the base plate and m_p is the mass of the plate.

These energy balance equations can be replaced by suitable equations that fit different types of collectors such as double-pass collectors,[95,96] parabolic trough collectors,[94] or evacuated tube collectors.[96] Various heat transfer coefficients may be evaluated as given in Duffie and Beckman,[106] Yamali and Solmus,[95] and Shabaneh et al.[107]

4.3.2 Humidifier Energy Balance

Here, h is the enthalpy and the subscripts in and out represent the inlet and outlet flows from each unit. The subscripts a and w refer to moist air and water, respectively,

$$\dot{m}_a[h_{a,out}(t) - h_{a,in}(t)] = \dot{m}_{w,in} h_{w,in}(t) - \dot{m}_{w,out}(t) h_{w,out}(t) \tag{4.4}$$

4.3.3 Dehumidifier Energy Balance

$$\dot{m}_a[h_{a,in}(t) - h_{a,out}(t)] = \dot{m}_{w,in} c_{p,w}[T_{w,out}(t) - T_{w,in}(t)] + \dot{m}_c(t) h_c(t) \tag{4.5}$$

The subscript c refers to the condensate (i.e., the product or desalinated water).

The determination of the outlet states for a humidifier or dehumidifier will in general require integration of the heat and mass transfer equations stepwise through the device. This is a cumbersome process for the investigation of cycle configuration, and so a different method based on component effectiveness has been developed by Narayan et al.[108] Effectiveness for a simultaneous heat and mass exchanger has been defined as the ratio of actual enthalpy change of either stream (air or water) to maximum possible enthalpy change:

$$\varepsilon = \frac{\Delta H}{\Delta H_{\max}} \tag{4.6}$$

Therefore, for the humidifier, for $\Delta H_{\max,w} < \Delta H_{\max,a}$,

$$\varepsilon = \frac{\Delta H_w}{\Delta H_{\max,w}} = \frac{\dot{m}_{w,in}h_{w,in} - \dot{m}_{w,out}h_{w,out}}{\dot{m}_{w,in}h_{w,in} - \dot{m}_{w,out}h^{ideal}_{w,out}} \tag{4.7}$$

$$\varepsilon = \frac{\Delta H_a}{\Delta H_{\max,a}} = \frac{\dot{m}_a h_{a,out} - \dot{m}_a h_{a,in}}{\dot{m}_a h^{ideal}_{a,out} - \dot{m}_a h_{a,in}} \tag{4.8}$$

By specifying the effectiveness of the component, the outlet states may be determined by control volume balances without a detailed numerical integration over the device. This is an on-design approach, and to establish the size of the desired device, an off-design analysis would subsequently be required (for fixed inlet states and effectiveness, counterflow humidification may not always be possible).

The system performance is expressed in terms of the GOR, given by:

$$\text{GOR} = \frac{\dot{m}_{product}h_{fg}}{Q_{in}} \tag{4.9}$$

4.4 Comparison, Limitations, and New Trends

Several investigators reported review papers related to HDH desalination systems such as Goosen et al.[109] and Narayan et al.[84] Since then, considerable progress has been achieved that represents new trends for increasing the GOR.

A solar still has a GOR of about 0.5, air-heated HDH cycles have a GOR that ranges from 1.7 to 3 (refer to Table 3), whereas the water-heated cycles have a GOR that ranges between 0.3 and 4.5, as indicated in Ref. 86. Various studies indicate that the top water temperature is an important parameter that influences the GOR, as is the mass flow rate ratio of the air and water streams as indicated in several recent studies.[112–115] Packing material quality plays a more important role in the system performance of air-heated cycles than for water-heated cycles. The multistage air-heated cycles have higher productivity but not necessarily high GOR. Comparing these GOR values with conventional desalination systems such as RO (equivalent GOR = 35–45 based upon an assumed efficiency of electrical generation), MSF (GOR of about 8), and MED (GOR up to 12) indicates that there is still room for improvement for HDH cycles to attain comparable gain output ratios. Some of these ideas are listed below.

Other arrangements that have been considered for improvement of the HDH process include the use of direct contact dehumidifiers as proposed by Khedr[110] and by Klausner and Mei[111] (referred to as diffusion-driven desalination, DDD), although the increase in GOR is not strong. Another improvement in the solar air-heated cycle is achieved by placing the solar heater after the humidifier (Narayan[112]) so that saturated air leaving the humidifier would be heated and then sent to the dehumidifier. This somewhat counterintuitive change results in a GOR of about 3.5.

Another set of suggested improvements to the cycle involves pressure variations, as proposed by El-Sharqawy et al.[116] and Narayan et al.[117] In one instance, the cycle operates at low pressure, since the humidity ratios are higher at low pressures as shown in Fig. 17. A further improvement is obtained by operating the humidifier at low pressure and the dehumidifier at slightly higher pressure. The two-pressure cycle is shown in Fig. 18.

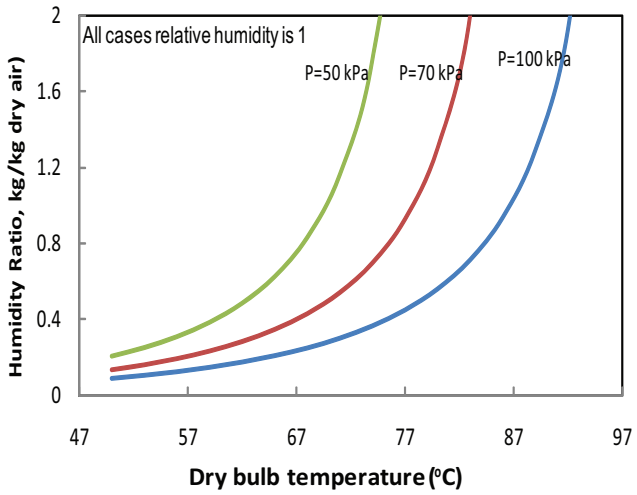

FIG. 17: Humidification at low pressure.[114]

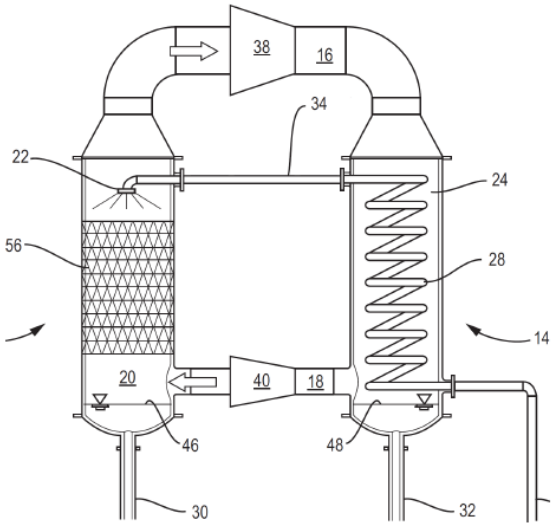

FIG. 18: Varied pressure cycle.[115]

Depending upon the form of the compressor (mechanical or thermocompression), the GOR can be well above 5 for this cycle.

Furthermore, extraction or injection of air or water between the dehumidifier and the humidifier can result in a decrease in the entropy generated within the system.[112] (For water-heated cycles without extraction, the top GOR is about 2.5, whereas a value of 4.5 refers to Muller-Holst's multiextraction case[86]) The extraction process—either single or multiple extraction—brings the modified heat capacity ratio HCR $= \Delta\dot{H}_{\max,a}\,/\Delta\dot{H}_{\max,w}$ closer to unity as shown in Fig. 19, resulting in a reduced entropy generation and accordingly, a higher GOR. A cycle with water heating and multiple extractions is shown schematically in Fig. 20.

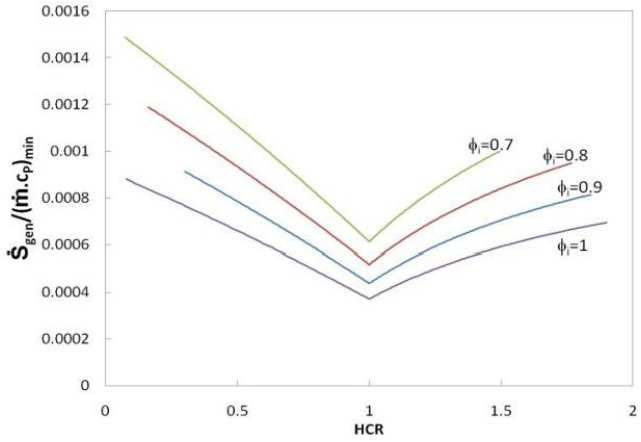

FIG. 19: Entropy generation in humidifier versus heat capacity ratio for various inlet relative humidities.[113]

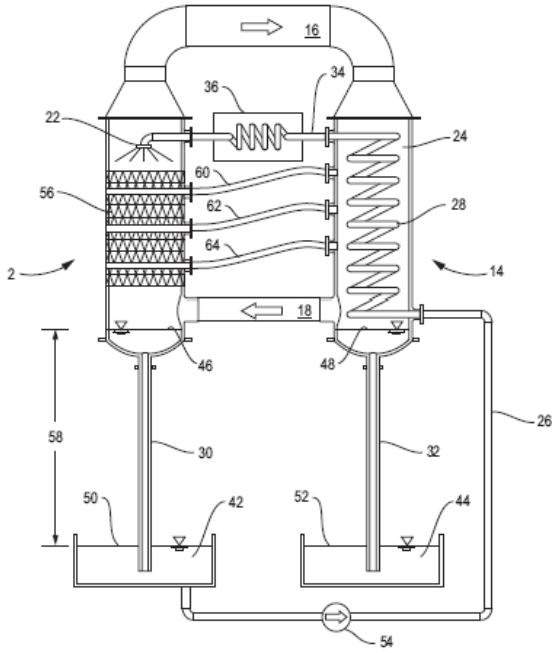

FIG. 20: Multiextraction water-heated cycle.[115]

4.5 Summary Comments on HDH

Current research trends have achieved substantial improvements in the GOR of the HDH system, but lower specific energy consumption is needed to compete with RO and conventional desalination techniques on an energy use basis. The HDH system remains attractive for small-scale deployment in the developing world, owing to its potentially low maintenance requirements and low capital investment. Considerable research is currently in progress in this regard.

5. SOLAR-DRIVEN MEMBRANE DISTILLATION

5.1 Introduction

Membrane distillation (MD) is a thermally driven separation process of aqueous solutions that involves the transport of vapor molecules through a hydrophobic microporous membrane. The membrane supports a vapor–liquid interface at the pores; the surface tension forces of the hydrophobic membrane prevent liquid molecules from entering the pores, while vapor passes due to a difference in vapor pressure at both sides of the membrane. The latter is established by a difference in temperature.

The main advantage of MD is that it operates at lower pressures than other separation processes based on membranes, since the driving force is not a difference in hydrostatic pressure. Typical operating pressures are on the order of zero to a few hundred kPa. Also, it operates at lower temperatures than conventional distillation, since it is not necessary to heat the liquids above their boiling point. Feed temperatures typically range from 60°C to 90°C, so low-exergy heat sources like solar energy are suitable for the process. Another advantage is the high efficiency in solute rejection, theoretically a 100% of nonvolatile components. This is achieved if the pores act efficiently as a barrier for the liquid phase, which requires that the liquid has low affinity for the membrane material (hydrophobicity). However, if the solution has surface active components, pore wettability can take place and allow liquid to pass to the other side of the membrane. Therefore, MD is mainly suited for applications in which the major component is water. Extensive reviews of the different MD applications (from concentrating water solutions to wastewater treatment) have already been published.[118−120] When using MD for desalination the main advantages are the lower operating pressure compared to other membrane-based processes, the possibility of obtaining purer water, and the ability to treat solutions with very high salinity.[121] In fact, MD is used to process brine effluents from other desalination processes in order to increase the recovery factor or even to obtain valuable salts in combination with crystallization.[122,123]

5.2 Fundamentals of Membrane Distillation

The vapor pressure difference across the membrane which drives the MD process can be established with different configurations (Fig. 21).

The most simple is when a solution colder than the feed is in direct contact with the permeate side of the membrane (direct contact membrane distillation, DCMD). The volatile molecules evaporate from the liquid–vapor interface of the warmer feed solution, pass through the membrane, and condense in the liquid–vapor interface created at the other side of the membrane by the cooling solution. However, the direct contact with the cool condensing solution significantly increases the sensible heat losses through the membrane. In order to diminish them, an air gap can be left between the permeate side of the membrane and a condensing surface in contact with the coolant solution (air gap membrane distillation, AGMD). The air gap increases the conductive heat transfer resistance of the membrane, but also the mass transfer resistance, so the permeation fluxes are lower. Larger temperature differences at both sides of the membrane can be applied to compensate for this deficit.

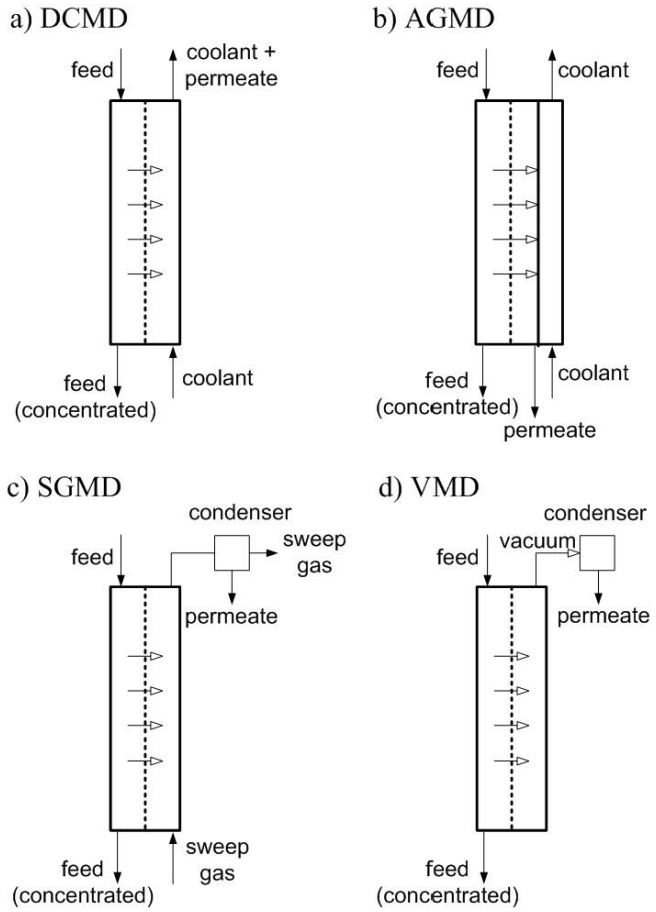

FIG. 21: Configurations of MD.

The reduced mass transfer resistance of AGMD can be avoided if a cold inert gas is used to sweep the permeate side of the membrane, carrying the vapor molecules so that condensation takes place outside the membrane module (sweeping gas membrane distillation, SGMD). The sweeping gas can be replaced by the application in the permeate side of a vacuum pressure lower than the saturation pressure of volatile molecules to be separated from the feed solution (vacuum membrane distillation, VMD). In this case the conductive heat losses through the membrane are reduced even more. However, the risk of membrane wetting is larger due to the higher pressure difference. The hydrostatic pressure across the membrane must not exceed the liquid entry pressure (LEP) of the pores, which has typical values between 1 and 4 bar for commercial membranes and depends on the surface tension of the feed but also on the physical properties of the membrane itself (material, pore size, etc.). Therefore, the membranes used in VMD have smaller pores (i.e., less than 0.45 μm diameter) than the ones used in other configurations.

Due to the hydrophobic nature of the membrane, a liquid–vapor interface is established at the entrance of each pore of the membrane. Water and volatile solutes from the feed so-

lution evaporate from this interface, diffuse across the pore, and condense on the other side of the membrane. Since no liquid transport occurs inside the pores, the diffusion of nonvolatile molecules is not possible and therefore they are rejected. In MD it is assumed that the vapor and the liquid are in the equilibrium state corresponding to the temperature at the membrane surface and the pressure within the pores. Mass transport takes place: (i) from the bulk feed to the membrane surface at the feed side in liquid form; (ii) through the pore in gaseous phase; and (iii) from the membrane surface at the permeate side to the bulk permeate in gaseous or liquid phase, depending on the configuration. Mass diffusion across the boundary layers next to the membrane limits the mass transfer. The concentration of nonvolatile solutes at the membrane surface becomes higher than at the bulk feed as the separation process takes place, creating a concentration polarization layer which increases the mass resistance and in extreme cases can lead to scaling on the membrane surface and wetting if the crystals break the hydrophobicity. Inside the pores, resistance to mass transfer comes from collisions between the diffusing molecules (molecular diffusion) or with the membrane itself (Knudsen diffusion), as well as the viscous drag from the membrane (Poiseuille flow).

Together with this mass transfer, heat transfer is established by the temperature gradient. Heat transfer from the feed solution to the membrane surface is usually the strongest limitation in the mass transfer, since the boundary decreases the heat supplied to the membrane surface for the evaporation. A temperature polarization effect takes place so that the bulk feed temperature is gradually decreased and therefore the temperature difference at the liquid–membrane interfaces is lower than that applied at the bulk phases. Heat transfer from the membrane surface to the bulk permeate side similarly creates a temperature polarization effect, although it depends on the configuration (in VMD, vacuum obviously prevents it). Across the membrane, the two most important heat transfer mechanisms are (i) conduction across the membrane matrix and the gas-filled pores (convection within the membrane pores is negligible); and (ii) transfer of latent heat of vaporization. The former is considered the main heat loss and should be minimized to increase the efficiency. The latter heat flow is unavoidable in MD, since it is the one associated with the mass transfer.

The parameter commonly used to evaluate the efficiency in thermal desalination processes is the GOR. As multieffect has rarely been contemplated in MD, the usual parameter considered is the more intuitive specific energy consumption, that is, the thermal energy added per unit volume of distillate produced.

Energy efficiency in MD is diminished mainly by: (i) polarization effects in temperature and concentration; (ii) mass transfer resistance within the pores; and (iii) conduction heat losses through the membrane. However, energy efficiency can be increased by heat recovery. In DCMD and AGMD, the latent heat of evaporation can be recovered by the coolant flow, which is preheated to be used as the feed flow on the other side of the membrane (in the latter case, heat from the distillate flow can also be recovered). In SGMD and VMD condensation takes place in an external condenser and the heat recovery depends on its efficiency. In the case of SGMD, heat recovery is more difficult since a small volume of permeate is vaporized in a large volume of sweep gas, which needs to be handled accordingly.

5.3 Operation and Performance

The effect of the different operating variables on the MD permeate flux for each configuration has been comprehensively reviewed[120,124] based on a long list of published papers, so only some basic results will be given here.

In all MD configurations, a linear increase in the permeate flux with the transmembrane vapor pressure difference is generally expected.

An increase in the feed temperature produces an exponential increase in the vapor pressure. However, the temperature polarization increases with the feed temperature as well and can mitigate the increase in permeate flux.

The effect of the feed concentration depends on the type of solution. When nonvolatile solutes increase, as is the case with desalination of saline water, the partial vapor pressure is reduced and the polarization effects increase, although the effect of the temperature polarization is usually more important.

The feed flow rate must be high enough to ensure turbulent flow (which increases heat transfer in the feed and reduces the concentration polarization effects) but not so much that the hydrostatic pressure of the membrane surpasses the liquid entry pressure of the feed solution into the pores.

In AGMD the most important parameter, together with the feed temperature, is the width of the air gap (about 10–100 times larger than the membrane thickness). Increasing the width reduces conduction losses but beyond 2 mm the mass transfer resistance due to the layer of stagnant air overcomes the increase in the energy efficiency.[125] The mass transfer resistance of the cold solution is small compared to the others. A decrease in the coolant temperature has a small effect on the distillate production and even smaller on the thermal efficiency. Only reducing the thermal conductivity of the membrane contributes to significantly improve the thermal efficiency of the process by reducing heat losses. This effect is less for membranes of high porosity, due to the larger volume of the pores compared to the solid matrix of the membrane.

In SGMD, both an increase in the velocity of the gas and a decrease of its temperature has a positive effect on the distillate production. However, there is a limit in the sweeping gas velocity, established by the pressure difference across the membrane (which must be smaller than the LEP). In VMD, the key factors for distillate production are the feed temperature and the vacuum pressure. Sensitivity to the former is stronger for larger vacuum pressure and to the latter for lower temperatures.

5.4 Characteristics of the Membranes and the Modules

The membrane must be hydrophobic and microporous. It does not need to be selective, since it acts just as a barrier, but it needs to show low resistance to mass transfer, high LEP for water, and low thermal conductivity, as well as thermal stability and chemical resistance.

The permeate flux increases with the porosity of the membrane and the size of the pores, and decreases with the membrane thickness and its tortuosity (relation between the average length of the pores and the membrane thickness). The typical size of the pores

ranges from 0.01 to 1 μm. The size is mainly determined by the requirement that the hydrostatic pressure across the membrane does not exceed the LEP of the pores. Smaller pores increase the mass transfer resistance. Usual values for the porosity are between 30 and 85%. High porosity decreases the conductive heat losses and offers large surface for evaporation. Membrane thickness increases the resistance to mass transfer but also decreases the conductive heat losses. Optimal thickness has been modeled to be between 30 and 60 μm. The general trend is that for larger thickness the permeate flux is lower except in AGMD, where the resistance of the air gap dominates that of the membrane thickness. For the membrane tortuosity a value of 2 is frequently assumed.

At the moment, no membranes are specifically designed for MD. As a result, those made for microfiltration are commonly used. Many are on the market, commonly made using polytetrafluoroethylene (PTFE), polypropylene (PP), and polyvinylidene fluoride (PDVF). Membranes used in MD modules can be flat sheet, tubular (capillary), or hollow fiber.[126]

Flat-sheet membranes can be arranged in plate-and-frame or in spiral-wound modules. The former require porous support plates and spacers. Several cassettes can be stacked together, each consisting of frames containing two membranes, intermediate feed channel for warm feed, and condensing walls. The whole stack is inserted between two end plates in an appropriate housing. Packing density, which is the ratio between the membrane area and the given packing volume, varies from 100 to 400 m^2/m^3, depending on the number of membranes used. In spiral-wound modules flow channels are made by spiral winding of membrane and condenser foils (Fig. 22). The packing density rises to 300–1000 m^2/m^3, depending on the channel height. The larger membrane surface allows high values of heat recovery and therefore a decrease in the thermal energy consumption, but the trade-off is a decrease in the specific production due to the reduction of the transmembrane temperature difference.

Tubular membranes are used in shell-and-tube membrane modules, which resemble shell-and-tube heat exchangers with membranes replacing the tubes through which a ra-

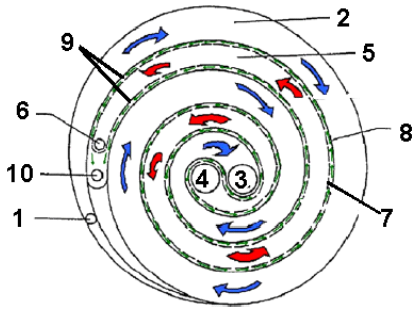

FIG. 22: Schematic diagram of the spiral-wound MD module concept with internal heat recovery. Cold brine enters at (1), circulates along condenser channel (2), and leaves preheated at (3). After receiving extra heat, it re-enters at (4), circulates along evaporator channel (5), and leaves at (6). Evaporation passes through the membrane (7), condenses on the condenser foil (8), and circulates along the distillate channels (9) before leaving the module (10). (Adapted from Ref. 131.)

dial mass flow takes place (Fig. 23). The diameter of tubular membranes typically varies between 1.0 and 2.5 cm, with a packing density of approximately 300 m^2/m^3. High velocities should be achieved in the feed to minimize polarization effects. In capillary modules, packing density increases to 600–1200 m^2/m^3 by arranging a large number of capillary membranes (inner diameter between 0.2 and 3 mm) in parallel as a bundle in a shell tube. In these cases, the membrane is an integral part of the modules and cannot be replaced, unlike flat-sheet membranes.

Hollow-fiber membranes (diameter 0.5 mm) provide the highest packing density (3000 m^2/m^3) but their softness and small fiber diameter make them susceptible to fouling and damage.

A well-designed membrane module should provide high rates of heat and mass transfer between the bulk solution and the solution–membrane interface, since in most cases the productivity of the MD process is limited by the heat and mass transfer resistances in the boundary layers. When coupling with solar energy, the operation differs from that at steady-state conditions in the laboratory with a constant source of heat, so heat recovery is very important to the productivity of the modules, even limiting the potential to raise plant capacity by increasing the membrane area.[127]

5.5 Experiences in Solar MD

There are many theoretical studies but few demonstration plants have been installed and analyzed (see Table 4). One of the first pilot experiences was in Australia.[128] The system consisted of a solar circuit (static solar collector and regulation tank) connected to a DCMD hollow-fiber module and an external heat exchanger for heat recovery. The system was found technically feasible and compatible with the transient nature of the solar energy. Heat recovery (60–80% required) had a very strong influence in the capital cost. Simulations resulted in values of the specific thermal energy consumption between 50 and 110 kWh/m^3 and distillate flow between 6.5 and 7.6 L/h m^2 of membrane. Experimental production rates were about 10% less. However, the calculated distillate production per unit collector area (17 L/d m^2 for Sydney in the summer) significantly improved on that of other solar distillation systems like solar stills.

The integration of a shell-and-tube MD module with a solar still was evaluated using the hot brine in the latter as feed.[129] The permeate flow showed a strong dependence on the temperature and flow rate of the feed and a very weak dependence on its salinity.

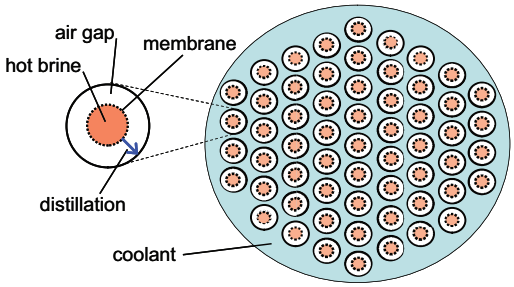

FIG. 23: Schematic diagram of a shell-and-tube AGMD module.

TABLE 4: Summary of experiments using solar MD for desalination. Shown for each case are type of module (h-f: hollow-fiber; s-t: shell-and-tube; s-w: spiral-wound; f-s: flat-sheet); membrane area (MA); membrane properties (ε: porosity; r: mean pore size; δ_m: thickness of the membrane; δ_g: air-gap width; d: internal diameter of hollow fiber; l: length of hollow fiber); specific thermal energy consumption (STEC) in kWh/m^3 of distillate; distillate flow (DF) in L/h m^2 of membrane surface; productivity in L/d m^2 of collector surface; and salinity of distillate.

Type of module	MA [m^2]	Membrane properties	STEC [kWh/m^3]	Dist. flow [L/h m^2]	Prod [L/d m^2]	Salinity [μS/cm]	Ref. no.
DCMD (h-f)	0.17	ε : 70%; r: 0.2 μm	50–110*	5.9–6.9	< 17	**	128
DCMD (s-t)	0.036	r: 0.2 μm δ_m: 1.5 mm	**	< 1.6	< 9	**	129
AGMD (s-w)	10	ε: 80% r: 0.05–0.2 μm δ_g: 30 μm	150–200	1–2.5	~ 9	< 10	130
AGMD (s-w)	10	ε: 80% r: 0.2 μm δ_g: 35 μm	200–300	< 2.5	< 19	< 5	132
AGMD (s-w)	4×10	ε: 80% r: 0.2 μm δ_g: 35 μm	200–300	< 1.5	2–11	40	133
AGMD (s-w)	5×10	ε: 80% r: 0.2 μm δ_g: 35 μm	Not given	1.5–1.6	< 13.3	Not given	134
AGMD (f-s)	2.94	Not given	**	< 5.5	**	5–30	135
AGMD (f-s)	3×2.8	Not given	810–2200	5–6.5	**	> 20	137
AGMD (f-s)	9	Not given	> 1805	< 3.2	**	2–5	139
AGMD (f-s)	3×3	Not given	294–379	3–5.1	**	2–5	139
VMD (h-f)	0.09	r: 0.1 μm d: 371 μm l: 0.14 m	7850	< 32.2	< 2	< 4	141

*Simulated.
**Not measured.

Another solar MD plant was constructed in the island of Ibiza (Spain), but using AGMD configuration with latent heat recovery integrated in a spiral-wound membrane module.[130] The additional mass transfer resistance associated with the AGMD configuration caused a reduction in the transmembrane flux and distillate flows were around 1–2.5 L/h m^2, with a thermal consumption of 150–200 kWh/m^3. Similar modules were devel-

oped by Fraunhofer-ISE (now marketed by Solarspring). A stand-alone MD system powered by solar thermal collectors specially conceived for solar desalination was designed and developed.[131] Simulation calculations showed that a very simple, compact system with a collector area of less than 6 m^2 could produce 120–160 L/d in the summer in a southern country. Several of those were developed in the framework of the EU project called SMADES.† Six compact systems (100–500 L/d) were installed and operated in different countries (Jordan, Morocco, Egypt, Germany, and Spain). The units had direct circulation of the feedwater through a 7 m^2 solar collector. Long-term performance tests demonstrated a durable operation even with very low maintenance. The compact system installed at the campus of the Jordan University of Science and Technology in Irbid, Jordan was comprehensively evaluated.[132] The specific thermal consumption (200–300 kWh/m^3) was less than half that of solar stills, while the daily production (19 L/m^2 of collector for 7 kWh/m^2 daily irradiation) was about 4 times larger. The recovery ratio (not larger than 4%) was worse than in other desalination systems (in MSF and MED figures are double and in RO can reach to 50%), although the quality of distillate was excellent: less than 5 μS/cm, despite high values (40 μS/cm) at the beginning of the operation which improved quickly with the production of distillate. Also, a larger system was designed with thermal storage and a heat exchanger to separate the solar and the desalination circuits. The system was installed in Aqaba, Jordan, working with seawater from the Red Sea, 72 m^2 of solar collectors and four MD modules operating in parallel, with an extended operation 6 h after sunset thanks to the heat storage tank. The production varied between 2 and 11 L/d m^2 of collector area.[133] A larger system (90 m^2 of solar collectors and five MD modules) was installed in Gran Canaria (Spain) but limited data are available.[134] The performance of the large systems seems slightly worse than for the compact systems, which shows the inefficiencies associated with the additional heat exchanger and the larger scale of operation.

A flat-sheet AGMD module was evaluated using thermal energy from a solar pond, taking heat from the bottom and using brine from the top of the pond as coolant.[135] Distillate flow reached maximum values of 5.5 L/h m^2 working with temperatures around 80°C and salinity of seawater. The investigation was based on the influence of the operational variables more than the energy efficiency or cost. A linear increase in the distillate flux with the transmembrane temperature difference was observed, as well as a significant decrease with increasing salinity and a weak dependence on hot side temperature. This latter fact and the continuation of flux at very low temperatures mean that the technology could take advantage of very low grade heat energy. However, leakage proportional to the pressure drop was encountered, which limited the pressure of the hot water passing through the module.

Similar AGMD modules, developed and manufactured by the Swedish company Scarab, were used in the context of the European project MEDESOL, where a solar multistage concept to minimize energy consumption was tried for seawater desalination.[136] A pilot plant was built consisting of three modules coupled with a static solar collector field. The performance of the system was analyzed as a function of operational variables and salt concentration.[137] Distillate production seemed not to be limited by vapor diffusion, as

†PV and thermally driven small-scale, stand-alone desalination systems with very low maintenance needs.

expected from an AGMD system, but by the transfer of heat, namely the heat transfer to the membrane surface, as would be the case of a DCMD system. A linear flux increase was observed with the temperature difference across the membrane, with only a slight dependence on the hot side absolute temperature. The modules showed specific distillate flux values up to a maximum of 6.5 L/h m^2 for a transmembrane temperature difference of 65°C and 1 g/L salt solution as feed. A productivity decay around 14% was observed with increasing salinity (from 1 to 35 g/L). The specific thermal energy consumption varied between 810 and 2200 kWh/m^3. Surplus thermal energy consumption in the range 100–400 kWh was observed for an increase in the salinity of the feed from 1 to 35 g/L. Apart from leakage problems faced during the experimentation, distillate conductivity got higher (i.e., from values < 10 μS/cm to average values of 40–60 μS/cm) with increasing salinity and lower transmembrane temperature difference, which correspond to the conditions for which the distillate flow decreases. Such low salt rejection values seemed to indicate that the membrane used was not the most adequate for desalination of seawater. As for the multistage concept, a general improvement of the efficiency was observed with increasing the number of stages but limited experimentation could be performed due to the module's continuous leakage.

The Memstill consortium developed another concept of AGMD configuring the module so that evaporation took place under ideal flow conditions, allowing for a high recovery of latent heat. Limited data exist on this technology and the operation of the pilot plants built to evaluate it. Researchers claimed that their modules had specific energy consumption between 22 and 66 kWh/m^3.[138] The technology, patented by Dutch company TNO, has been licensed to two companies that are now testing industrial fabrication processes of the modules, Dutch Aquastill and Singaporean Keppel Seghers. Several modules of the latter have been evaluated at PSA in Spain.[139] The latest was a module designed for a three-stage configuration in series. Tests were done for simulated seawater, feed temperature of 80°C, and cooling temperature of 30°C, and results showed a trade-off between the production and the energy efficiency. For the minimum operational value of the feed flow rate (10 L/min), the specific thermal energy consumption was the minimum (294 kWh/m^3) but also the distillate flow (3 L/h m^2). For the maximum value of the feed flow (twice larger), maximum distillate flow was reached (5.1 L/h m^2) but also maximum thermal consumption (379 kWh/m^3). The distillate was in all cases of very high quality (in the range of 2–5 μS/cm).

VMD has been proposed for desalination, and it has great potential based on calculations.[140] A recent study proved the feasibility of producing potable water from underground water by means of a hollow-fiber module coupled with a solar energy collector (n24). The largest permeate flux obtained was 32.2 L/h m^2 in an experiment with 0.09 m^2 of membrane area and an 8 m^2 solar energy collector in Southern China. However, the technology needs scaling up to become a feasible option. Theoretical investigations of seawater desalination by coupling solar energy and VMD recently showed that the use of solar collectors was more efficient than the coupling with a solar pond, predicting a maximum permeate flux of 142 L/h m^2 for a vacuum pressure of 500 Pa.[142] A semi-industrial pilot plant is now in operation in Tunisia using VMD and flat-plate solar collectors in order to verify the simulations against experiments. The Memsys Company also recently

launched another VMD module which delivers high flux and has a very good energy recovery by working in a true multieffect distillation (several evaporation/condensation stages). Demonstration plants are now being built.

In conclusion, the application of solar-driven membrane distillation for desalination is still a promising concept with only a few applications outside the laboratory and as yet on a very small scale. Although the performance in energy and productivity has been shown to be capable of improving on other small-scale processes like solar stills, the potential to compete with other solar thermal desalination technologies, such as multieffect distillation, is yet to be demonstrated.

6. SOLAR THERMAL COPRODUCTION OF WATER AND ELECTRICITY

6.1 Introduction

Due to the high energy consumption of desalination processes, large desalination plants are typically associated with or close to power production facilities. In the case of thermal desalination processes (MSF, MED), the plants are normally integrated into electricity production plants using steam extracted from a conventional Rankine cycle. In this context, the idea of integrating desalination in solar power plants is, therefore, very attractive as solar radiation is usually abundant in places where fresh water is scarce. With the current commercial development of CSP technology all over the sunny areas of the world, solar power-water cogeneration plants (CSP+D) appear as a possible means of sustainably reducing power and water problems in many arid and semiarid areas of the world.[143] This situation is clearly reflected in the MENA region (Middle East and North Africa), which has very large and important development of desalination and also a very high potential for CSP technology development and implementation; large projects, such as the Desertec Initiative and the Mediterranean Solar Plan, are currently underway.[144,146]

The concept of combining CSP and desalination facilities is a very attractive solution for the following reasons:

1. At many locations with high solar potential, combined water-power projects can be more attractive to local stakeholders than stand-alone power production projects.

2. Technological synergies can be identified to potentially reduce the cost of combined power and water production relative to the independent production of the same items.

3. Financial arrangements can also benefit, as water and power cost can be better adapted to the specific local conditions of the facility.

4. Politically, the exportation of electricity to other countries can be justified (in many cases, this is the only reasonable way to make the electrical projects bankable) and, at the same time, the basic needs of the local population can be addressed by locally distributing the water, partially financed by the sale of power.

However, the concept also has some drawbacks:

1. The CSP+D concept obviously needs facilities to be located near the sea, where land cost and availability can be a significant problem.

2. DNI (direct normal irradiation) is normally lower in the areas close to the sea.

3. Some technological aspects are not yet solved, and specific research, development, and demonstration activities are needed to define the best concepts and systems.[145]

6.2 Concentrating Solar Power Plants

The first commercial application of CSP technology occurred nearly 100 years ago in Meadi (near Cairo, Egypt) in 1912, when the American inventor Shuman developed and installed a parabolic trough collector system (5 rows of 62 m length $\times$ 4 m aperture each) to produce steam and drive a 120 HP steam turbine, in an effort to avoid the transportation of coal from England to Egypt.[147] However, real commercial development of solar power generation technology happened in the early 1980s in California (USA) with the construction of the first Solar Energy Generating Systems (SEGS): five 30 MW hybrid parabolic trough power plants totaling 150 MW capacity, commissioned in 1986–1988, were constructed in Kramer Junction and another four (Daggett, 14 and 30 MW, and Harper Lake, 2 $\times$ 80 MW), totaled a combined installed solar power of 354 MW.[148] The conceptual scheme of these plants, still in operation today, was the use of a large parabolic trough collector field (around 2.2×10^5 m^2 in the 30 MW plants and 4.7×10^5 m^2 in the 80 MW ones) to heat thermal oil, circulating by the absorber tube located at the focus of collector parabola, from 295 to 395°C (SEGS VI and VII). This heat transfer fluid was used to produce steam at 100 bar and 371°C, which was expanded in a conventional steam turbine producing power.[149]

After the SEGS plants, a period of 16 years followed with no commercial CSP activity until 2007, when the PS10 (Seville, Spain) and the Nevada Solar One (Las Vegas, NV) solar plants started their activity. After that many solar commercial projects followed, with Spain the most active country in the period 2007–2011 (2340 MW will be operative in that country, in about 60 CSP plants, by the end of 2013). Among all the CSP technologies that are in clear development (parabolic troughs, linear Fresnel, central tower, parabolic dishes), the present market dominance clearly corresponds to parabolic troughs. A second generation is currently being implemented based on a solar field of about 5×10^5 m^2 and the introduction of thermal storage based on molten salts to achieve a nominal power production of 50 MW with 7.5 h of thermal storage from the molten salts. Thermal storage, which does imply an important increase in the needed investment, provides power dispatchability (guarantee of power supply to the grid), which is a unique advantage, not existing with any other renewable energy technology to date. Additional advantages of thermal storage are to provide:

1. Higher potential value for the produced electricity, as the power can adapt to the demand and be dispatched at the request of power grid operators.

2. Lower cost, as thermal storage in CSP power plants is cheaper than turbine capacity increase and allows the use of all collected solar energy.

3. Grid stability, as the plant is not affected by abrupt changes into the output power, as is very common in PV plants.

4. Higher plant capacity factor (ratio of the actual output of the plant over a period of time to its potential output if it had operated at full *nominal capacity*), which directly translates into lower electricity costs.

The current-state-of-the-art thermal storage for CSP plants is based on a eutectic mixture formed by 60% of sodium nitrate and 40% of potassium nitrate.[150] This mixture has a fusion temperature of 221°C. In a typical 50 MW plant, 2.85×10^4 tons of these salts are used (nominal storage capacity of 1010 MWh_{th}) to get the equivalent of about 7.5 h of nominal power generation.[151] The indicated mixture is used because it has the following advantages:

1. High density of energy storage (per unit of mass and volume) with reduced thermal losses.

2. Good heat transfer performance and mechanical and chemical stability.

3. Chemical compatibility with the conventional heat transfer fluid (synthetic oil).

4. High number of heat charge–discharge cycles with low degradation velocity.

5. Good relationship between heat storage capacity and cost.

6. Very low vapor pressure at working temperatures.

7. Contains neither flammables nor contaminants (the salts are normally used as fertilizer) and it is easily managed.

With regard to parabolic trough technology, current designs are based on either LS-3 or Euro-Trough-type developments, using a parabola aperture of about 5.7 m and lengths between 100 and 150 m per individual collector. Optical efficiency is around 80%, without considering any ancillary zones such as expansion bellows, supports, glass–metal union items, etc.

Third-generation parabolic trough power plants are currently under development with the start of construction in the US of several CSP plants with nominal capacity in the range of 250 MW. This higher size is expected to significantly reduce the electricity generation cost.

6.3 Integration of Multieffect Distillation and Reverse Osmosis Desalination Technologies into Concentrating Solar Power Plants

Studies of different basic integrated power and desalination plant configurations have been published, such as the description of the operation of low-temperature multieffect distillation (LT-MED) desalination plants using low-grade steam from different power plants.[152] Other studies address the energy cost analysis to produce water from an integrated power plant into LT-MED and thermal vapor compression MED (TVC-MED) units,[153] evaluate

the benefits of integrating RO units with existing power/desalination plants in the Middle East,[154] or perform thermoeconomic analysis of different configurations for the combination of a reverse osmosis subsystem to produce drinkable water and a steam power plant to generate electricity.[155] Considering the specific case of CSP+D plants, some studies show the potential of CSP plants coupled with desalination systems (RO and MED) for deployment in the MENA region,[156] and other studies technoeconomically analyze the combination of parabolic trough power plants for electricity production with MED and ultrafiltration/RO plants.[157,158]

When the possible options to combine power production and desalination in dual-purpose plants are analyzed, the best options are MED and RO. This is because these are, respectively, the most efficient thermal and electrical desalination technologies. In the case of RO the integration is a straightforward issue by simply using the produced electricity to feed the desalination unit. In addition, the power and desalination plants do not need to be physically close to each other, a fact that could impart a significant advantage due to the previously mentioned inconvenience that DNI is normally lower at the areas close to the sea. Thus, the solar power plant can be placed at better inland locations and the RO desalination plant can be by the sea, minimizing seawater pumping requirements.

If a cold water source of about 30°C (or lower) is easily available for the cooling process of the power cycle, then the option of RO would always be the preferred one. This is because in this case the expansion in the steam turbine can be made up to 0.07 bar (about 40°C), so that the penalty of any steam extraction to drive a MED desalination process would be very high, making the RO technology more energy efficient. One recent study which considered the case of Cyprus confirms this conclusion.[158]

The second option, CSP and MED facilities, is based on the use of low-grade steam from the power cycle (typically a Rankine one) to provide the thermal energy needed by the desalination process. This means that the MED unit needs to be physically located close to the steam turbine. The first, immediate inconvenience is that distance to the sea must be carefully analyzed to optimize and balance the global power and water production output (direct function of DNI potential), the pumping energy requirements, and the initial capital investment. This combination provides additional advantages such as reducing or eliminating the cooling requirements of the power cycle by using the desalination MED process to partially (or completely) replace the conventional cooler associated with the power block. In addition, challenging ambient conditions in specific regions, such as the Middle East/Persian Gulf with seasonal high seawater temperatures and saline concentrations, imply the necessity to increase the temperature level at turbine exhaust steam output to make cooling feasible. In these conditions, the penalty to power production that results from using steam to drive an MED process is substantially reduced, and it is, from a thermodynamic point of view, very attractive against the RO option, which is normally heavy penalized when high salinity water is used, from both the energy and maintenance points of view.

When integration of CSP and MED technologies is analyzed, two different types of configurations can be considered: using the exhausted steam from the CSP plant as the source of the heat (LT-MED), and a novel system consisting of a low-temperature multi-effect distillation plant powered by the steam produced from a thermal vapor compressor

(TVC). In this case, unlike a typical TVC-MED process, the vapor to be used in the steam ejector comes from the exhausted steam of the CSP plant instead of an intermediate effect of the desalination unit. This new concept (LT-MED-TVC) has a strong potential since it is useful for the coupling of any thermal desalination process to a CSP plant, as different schemes can be considered depending on the quality (pressure) of the steam extracted from the low-pressure turbine, to be used as the motive steam in the ejector. Figures 24 to 26 show the systems under consideration:

1. Configuration 1: LT-MED unit integrated into a PT-CSP plant (Fig. 24).
2. Configuration 2: LT-MED-TVC unit integrated into a PT-CSP plant with steam extractions in the low-pressure (LP) turbine (Fig. 25).
3. Configuration 3: RO unit connected to a PT-CSP plant (Fig. 26).

As can be observed in the figures, the thermal energy from the solar field in all configurations is exploited by a power conversion system consisting of a preheater, an evaporator, and a superheater. The resulting steam is sent to a high-pressure turbine where it expands before being reheated and expanded again in a low-pressure turbine, producing power. The configuration shown in Fig. 24 consists of an LT-MED unit integrated into a PT-CSP plant. In this option, the desalination plant is directly fed by the low-temperature steam from the turbine outlet, with the MED unit acting as the cooler of the power plant.

In the second configuration (Fig. 25), a steam ejector uses part of the exhaust steam from the turbine to provide the energy needed by the MED unit. With this scheme, different possible configurations can be achieved, depending on the enthalpy of the steam extracted to be used as motive flow in the ejector. The resulting compressed vapor is injected into the first effect of the distillation unit. A dry cooling system is considered for condensing the remaining exhaust steam from the turbine. This cooling option is usually the one selected in arid areas, since typical wet cooling towers consume between 2 and 3 metric tons of water per MWh of produced electricity.[160] The use of seawater as a cooling option (sensible heat) would imply a higher (than dry cooling) energy consumption, due to the large amount of water that would need to be pumped and the distance from the sea that the whole facility is likely to be located (from about 2 to 5 km).

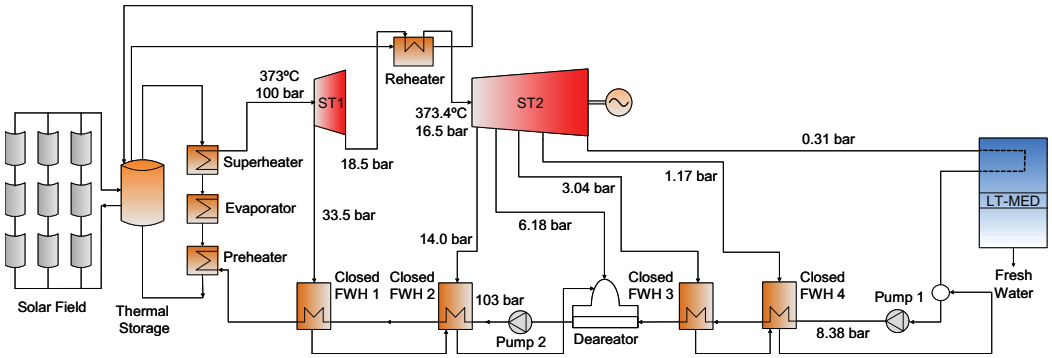

FIG. 24: Diagram of the LT-MED unit integration into a PT-CSP plant.

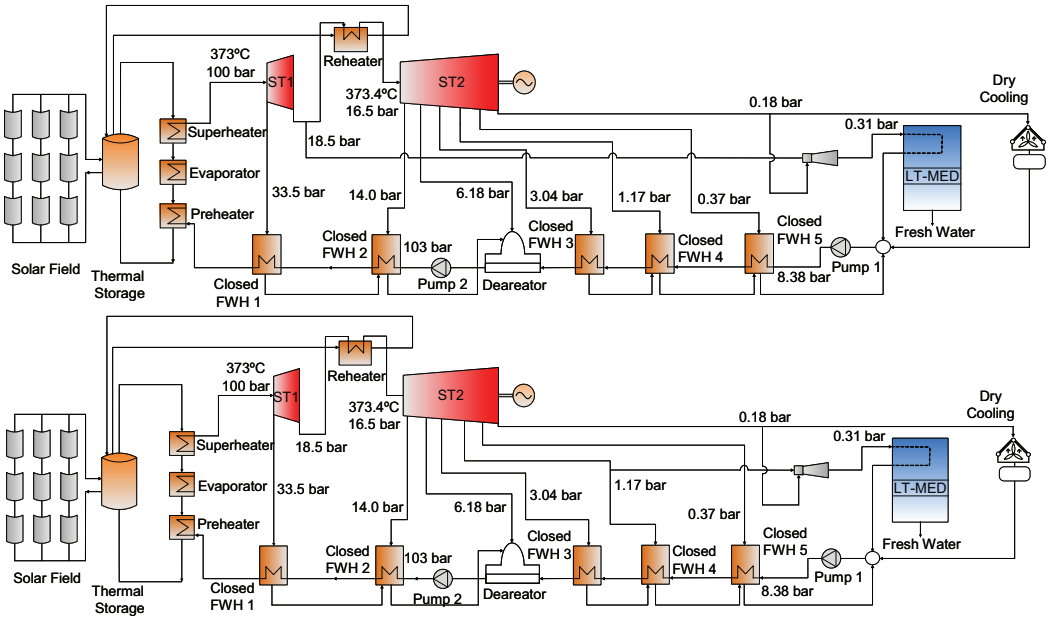

FIG. 25: Diagram of the LT-MED-TVC unit integration into a PT-CSP plant (two of several possible configurations).

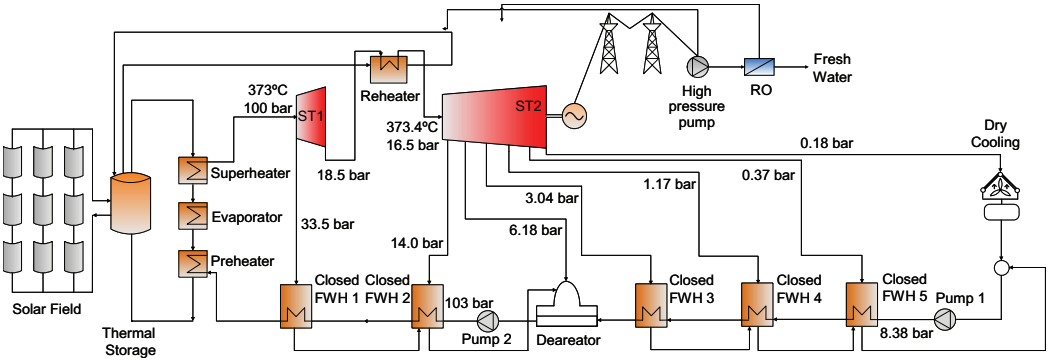

FIG. 26: Diagram of the RO unit integration into a PT-CSP plant.

Finally, in the third configuration (Fig. 26), the RO plant is driven by the power output from the PT-CSP plant.

Operating conditions of the solar power plants shown in the previous configurations (Figs. 24 to 26) were taken from the power cycle of Andasol-1 plant,[161] which was the first commercial CSP plant to introduce a molten salt thermal storage system.

6.4 Case Study: Port Safaga (Egypt)

To determine the efficiency of these different configurations, a thermodynamic analysis using a steady-state computer model is needed. This can be done by assessing the net

thermal output capacity (which is the thermal power required by the power cycle, provided by the solar field), the overall efficiency, and the cooling requirements. This yields a set of nonlinear, algebraic equations for each thermodynamic cycle and the steady-flow energy equations of all the components associated with the power cycle (pump, reheater, heat exchanger, condenser, turbine, etc).

This study was performed for the specific location of Port Safaga in Egypt (Red Sea), which can be considered as a representative case in the Middle East and Persian Gulf region. A DNI value of 2496 kWh/m^2-yr was estimated for this location from satellite images. In all cases, a net CSP plant power production of 50 MWe was considered, since this is a typical size of most existing solar plants. This means that all internal electrical consumptions (pumps, desalination unit, dry condenser, etc.) are considered and deducted to achieve the net production of 50 MWe. The following parameters, assumptions, and boundary conditions have been taken into account in the computer model:[162]

- Plant location: Port Safaga (Egypt) (longitude 33.81° E; latitude 26.79°N).
- Design point: 27 September (radiation at solar noon 968.99 W/m^2, 36.89°C).
- Parabolic trough solar field based on the LS-3 type collector.
- North–South orientation (of parabolic trough collectors). Main characteristics: 99.0 m longitude, 545 m^2 of aperture area, 0.76 of peak optical efficiency.
- Distance to the sea of CSP+D facility: 3 km.
- Thermal storage (molten salts) system for 24 h solar operation at design day. This implies an equivalent thermal storage capacity of about 13 h, with possibility to run 24 h from midspring to midautumn.
- Thermal oil (heat transfer fluid) type: Monsanto VP-1.
- Inlet temperature to the field: 295°C.
- Outlet temperature from the field: 390°C.
- Actual expansion and compression processes have been considered.
- An isentropic efficiency of 0.852 has been taken for the high-pressure steam turbine, and an isentropic efficiency of 0.85 for the low-pressure steam turbine.
- An isentropic efficiency of 0.75 has been taken for the pumps of the power cycle.
- Dry cooling is used for the power cycle steam condensing but seawater is used in the case of MED cooling. This is due to the large amount of seawater that would be needed to pump in the case of Rankine cycle, which would significantly increase pumping energy consumption.
- Condensing conditions at LP turbine (configuration 1): 70°C (0.31 bar), as needed by the MED unit.

- Condensing conditions at LP turbine (configurations 2 and 3): 58°C (0.18 bar). This is a consequence of high ambient temperatures and the use of dry condensers.[163]
- Condensing temperature of MED last effect: 40°C (seawater temperature at 30°C).
- A specific electric consumption of 2.11 kWh/m^3 has been assumed in the case of an MED plant (this figure includes the pumping consumption of needed seawater, including MED cooling requirements) and 5.46 kWh/m^3 in the case of RO, which are the estimated values for the selected Egypt location.[156]
- The GOR has been assumed to be 8.4 in all cases of MED plant.
- The power required by the cooling unit has been taken from a study of a dry-cooled parabolic trough plant located in the Mojave Desert, which showed 5% less electric energy produced annually.[160]
- When not all the steam from an LP turbine is taken to the condenser, the energy consumption estimated by the dry cooling system is proportionally lower.

In all analyzed cases, nominal desalination plant production was 3.5×10^4 m^3/day, an amount defined by the configuration PT-CSP + LT-MED (configuration 1) when all the steam from the turbine outlet at 70°C feeds the MED unit. With these data, several thermodynamic simulations have been performed for the LT-MED-TVC and RO configurations (configurations 2 and 3, respectively). In the case of configuration 2, the simulations have been performed using part of the steam that is extracted from the low-pressure turbine (at pressures 1.17, 3.04, 6.18, and 14.0 bar) as motive steam. Table 5 shows the results of the thermodynamic analysis for all configurations, calculating the total thermal energy required by the integrated power and desalination facility (provided by the thermal storage system), cooling requirements, the solar field size needed according to the DNI potential of the selected location, and the overall combined facility efficiency, always considering the same net power and water production (50 MWe and 3.5×10^4 m^3/day, respectively).

With defined conditions, the integration of an LT-MED unit into a PT-CSP plant gets the best results, which means that the reduction of power production for this configuration due to the higher pressure of the exhaust steam is less than the extra power that the

TABLE 5: Main data of different CSP+D configurations analyzed to Port Safaga (Egypt) case study (50 MWe and 35.018 m^3/day in all configurations)

	Desalination system	**Thermal energy consumption (MW_{th})**	**Cooling requirements (%)**	**Parabolic trough field area (m^2)**	**CSP+D efficiency (%)**
Conf. 1	LT-MED	161	0	733,570	31.1
Conf. 2	LT-MED-TVC (1.17 bar)	180	19	824,040	27.7
	LT-MED-TVC (3.04 bar)	191	27	872,000	26.2
	LT-MED-TVC (6.18 bar)	198	30	905,790	25.2
	LT-MED-TVC (14 bar)	208	34	948,300	24.1
Conf. 3	RO	175	100	798,970	28.6

CSP must generate in configuration 3 for RO desalination process. In addition, no power plant cooling would be required in this configuration and therefore no condenser would (theoretically) be necessary.

LT-MED-TVC configurations show worse results than configurations 1 and 3, as it uses a high-exergy steam to feed a steam ejector which provides the steam required by the MED desalination process. However, it has the advantage over the RO configuration of lower cooling requirements. In addition, when compared to the first configuration, the integration of an LT-MED into a PT-CSP plant by replacing the cooling unit has a major disadvantage in the fact that the desalination plant must be very close to the turbine since the exhaust steam has very low density, and therefore pipes with very large diameters are needed to conduct the steam to the desalination plant. This is why the thermal compression of the steam (LT-MED-TVC) can also be considered as a feasible option.

6.5 Cost Estimates

To estimate the power and water costs of the more efficient configurations from the previous case study described (PT-CSP/LT-MED and PT-CSP/RO), the following definition of levelized electricity cost (LEC) can be used:[164]

$$\text{LEC} = \frac{crf \times K_{invest} + K_{O\&M} + K_{fuel}}{E_{net}} \tag{6.1}$$

$$crf = \frac{k_d\,(1 + k_d)^n}{(1 + k_d)^n - 1} + k_{insurance} \tag{6.2}$$

where $k_{insurance}$ is annual insurance rate (typical value = 1%), K_{invest} is total investment of the plant, K_{fuel} is annual fuel cost (not applicable in the case of solar energy without backup); k_d is real debt interest rate (value used = 8%), n is depreciation period in years (value used = 25 years), $K_{O\&M}$ is annual operation and maintenance costs, and E_{net} is annual net electricity delivered to the grid.

Additional data used to calculate the cost of the solar power are the following:

1. From a practical point of view, a CSP plant is considered with 13 h of thermal storage, working 24 h from midspring to midautumn, and also at nominal turbine capacity the rest of the year.
2. Investment cost of the 50 MW PT-CSP plant without thermal storage: 3300 €/kW-nominal.
3. Investment cost of thermal storage: 40 €/kWh-stored.
4. About 200 hectares of flat land needed.
5. Plant availability: 96%.
6. Consumption for the cleaning of the mirrors: 0.07 m^3/MWh_e.[165]
7. Land costs are not considered.

The same procedure will be used to estimate the levelized water cost (LWC). Additional data to calculate the cost of the desalination plant:

1. Investment cost of RO facility: 850 €/m^3 day installed (availability: 92%).
2. Investment cost of MED facility: 1050 €/m^3 day installed (availability: 98%).
3. Specific electricity consumption by RO plant: 5.46 kWh/m^3.
4. Specific electricity consumption by MED plant: 2.11 kWh/m^3.
5. Chemical consumption, manpower, membrane replacement, spare parts, and all other fixed and variable costs were also considered.

The main cost results are summarized in Table 6.

6.6 Summary Comments on Coproduction

Solar thermal coproduction of water and electricity can only be made at large CSP plants, with RO and MED the two most reasonable options for desalination technology. Under the considered hypothesis and scenarios, the RO option would be more efficient in most cases, having also the advantage of not constraining the geographical location of the solar plant, potentially avoiding typical problems of land availability and lower DNI levels close to seashore.

However, when ambient temperatures drastically limit the expansion at steam turbines and the only reasonable solution to exhaust steam condensing is dry cooling, there is some room for a more energy efficient, and maybe even more economical, MED option. The results have shown that, at 0.18 bar in the turbine outlet conditions, the configuration that involves LT-MED is more efficient thermodynamically than the coupling of the CSP plant with an RO desalination plant and needs a smaller solar field for the same production of electricity. Moreover, this configuration has the advantage of not requiring any power plant cooling. The results obtained are valid for arid regions, where RO has higher specific electric consumption and dry cooling is used in CSP plants; and, coincidentally, nearly all locations in which thermal desalination technologies have an important market (Middle East and Persian Gulf region) have these constraints.

TABLE 6: Comparative costs of power (50 MWe nominal net production) and water (40,520 m^3/day nominal net production) cogeneration with PT-CSP/RO and PT-CSP/LT-MED configurations

Cogeneration system	Investment solar plant (M€)	Investment desalination plant (M€)	LEC (€/kWh)	LWC (€/m^3)
PT-CSP / RO	406.76	29.83	0.178	0.649
PT-CSP / LT-MED	380.38	36.84	0.169	0.706

Finally, a novel configuration of MED plant with thermocompression, named LT-MED-TVC, can also be considered. This configuration requires a larger solar field than the combination of CSP + RO when the motive steam comes from the high-pressure turbine. However, the energy losses to the ambient are lower for this configuration, since the plant cooling needs decrease from the CSP + RO case. Simulations show that more efficient thermodynamic configurations can be achieved at lower pressures of steam extractions from the low-pressure turbine. In the case of pressure values slightly higher than 1 bar, the results obtained in the integration of the LT-MED-TVC desalination unit into the CSP plant are very similar to those obtained with CSP + RO.

7. PHOTOVOLTAIC POWERED DESALINATION SYSTEMS

7.1 Introduction

Previous sections have discussed the use of solar thermal energy to desalinate water. In this section, systems which convert solar radiation into electricity using photovoltaics are reviewed. For both seawater and brackish water desalination, photovoltaic reverse osmosis (PVRO) systems have been developed.[170−177,179,183,185,189−201] For brackish water desalination, photovoltaic electrodialysis (PVED) has been explored.[202−206] Both of these systems have the potential to provide clean water to remote and water-stressed areas.

Here, we provide an overview of the PVRO and PVED approaches. First, the fundamentals of photovoltaic operation and their performance limits are reviewed. Next, the technical details and fundamental challenges of the two systems are described. Finally, cost considerations for photovoltaic-powered desalination systems are presented.

7.2 Overview of Photovoltaic Performance

7.2.1 Photovoltaic Devices

Photovoltaics convert light energy directly to electrical energy when photons raise electrons in a semiconducting material from the valence band to the conduction band. Photovoltaics have many advantages such as no moving parts, free energy, and simple operation and maintenance. As with solar thermal systems, once set up, solar photovoltaic systems have no greenhouse gas emissions.

A PV cell is composed of two or more layers of doped semiconducting materials. When exposed to sunlight, electrons are excited and conducted by electrical contacts to an external circuit. A typical PV cell produces only a few watts of power. Cells are typically strung together in series and are encapsulated in a PV module to provide adequate voltage. These modules are then strung together in array to provide enough power for a given application.

Due to the bandgap of the semiconductor, photovoltaic cells can only convert a portion of the solar spectrum into electrical energy. The remainder of the solar energy is lost to heat. Conversion efficiencies of photovoltaic cells vary depending upon the material and process used to produce the cells. Many different types of semiconducting materials are used in PV cells. The majority of commercial PV modules on the market today are made of silicon (Si), which can be divided into three main categories: monocrystalline silicon, which is

the highest efficiency and cost, polycrystalline silicon, which has a less ordered crystal structure and lower efficiency, and amorphous silicon, which is a thin-film technology with relatively low efficiency. Other compounds that are commonly used in solar cells include cadmium telluride (CdTe), gallium arsenide (GaAs), and copper indium gallium selenide (CIGS). Common efficiencies for commercial monocrystalline silicon modules are 15–18%. The highest observed conversion efficiency of 42.3% was for a multijunction GaAs concentrator solar cell.[166] Some common and the best observed conversion efficiencies for the different technologies are listed in Table 7.

7.2.2 Solar Panel Model

The basic operation of a solar cell can be represented using the classic one-diode model. In this model, depicted in Fig. 27, the current produced by a solar module is given by Ref. 167:

$$I = I_{ph} - I_0 \left[\exp\left(\frac{V + IR_s}{nkT_{cell}/q} \right) - 1 \right] - \frac{V + IR_s}{R_{sh}} \tag{7.1}$$

where I_{ph} is the light generated current, I_0 is the reverse saturation current which is affected by temperature, V is the panel operating voltage, I is the operating current, R_s is the panel series resistance, R_{sh} is the panel shunt resistance, n is the diode ideality factor, k is the Boltzmann constant, T_{cell} is the cell temperature, and q is the charge of the electron. Note that I_0, R_s, R_{sh}, and n are all panel specific parameters. The light generated current can be represented by

$$I_{ph} = A_{panel} \left(C_0 + C_1 T_{cell} \right) G_{rad} \tag{7.2}$$

where A_{panel} is the area of the solar panel, G_{rad} is the incoming solar radiation normal to the cell, and C_0 and C_1 are panel specific constants.

TABLE 7: Terrestrial single-junction solar module conversion efficiencies

Technology	**Common conversion efficiency**[207]	**Best observed conversion efficiencies**[166]
Silicon		
Monocrystalline	15–18%	21.4%
Polycrystalline	12–16%	17.5%
Amorphous	6–8%	8.2%
CIGS	10–14%	15.7%
CdTe	8–11%	10.9%

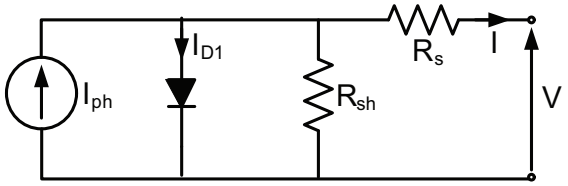

FIG. 27: Electrical circuit representation of the five-parameter solar module model.

From the above equations, the output current of the photovoltaic module is dependent on many factors including the operating voltage, the solar radiation, and the solar cell temperature. A typical solar panel output current and power for different operating voltages and levels of solar radiation are shown in Fig. 28. In these figures, for each solar radiation level, there exists an operating voltage for which the solar panel produces the maximum amount of power. In general, connecting a load directly to a solar panel will not result in the voltage that gives maximum power output. Typically a power converter with a maximum power point tracking algorithm is required to optimize the power output.[168]

Temperature is also an important factor affecting the performance of PV panels. The variation in power output with temperature of a typical PV panel for a given level of solar radiation is shown in Fig. 29. Temperature has a substantial effect on the power output of the panel; increasing the temperature by one degree Kelvin results in a 0.4% decrease in power output for silicon solar panels.[167] Temperature also greatly affects the position of the optimal operating point. A maximum power point tracker is required to ensure the panel output is optimized. Both of these effects must be considered when designing a photovoltaic powered desalination system.

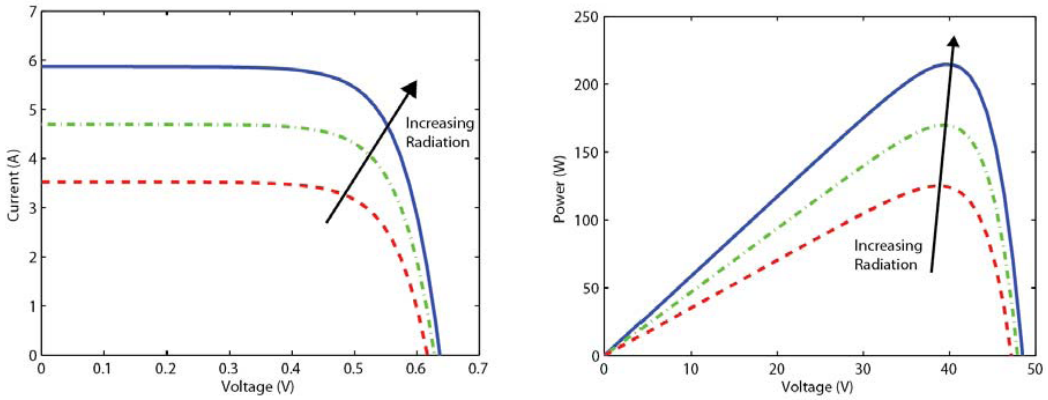

FIG. 28: Typical photovoltaic panel operating curves.

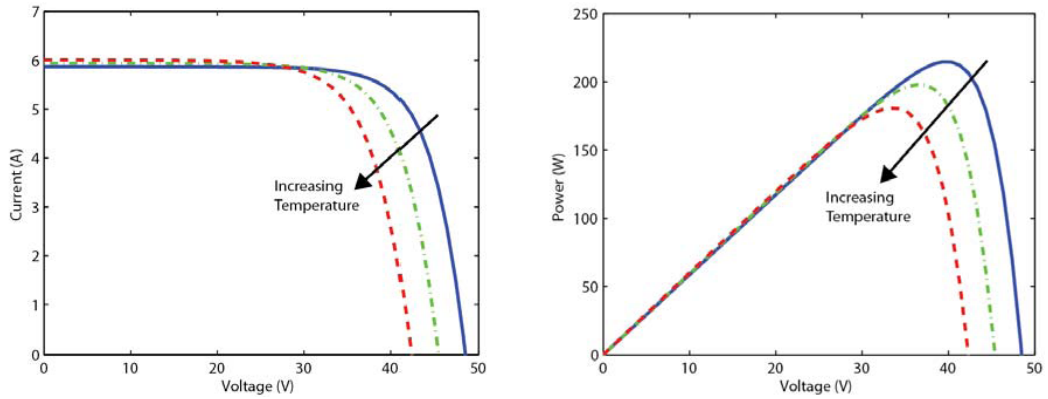

FIG. 29: Variation in solar panel performance with variation in cell temperatures.

7.3 PVRO Systems

Reverse osmosis systems can be coupled to PV panels to desalinate water. PVRO systems have many different configurations. A simple reverse osmosis system with energy recovery and batteries is shown in Fig. 30. In this system, the control electronics direct power from the PV panels and the battery to the pumps to pressurize the incoming water. The water is driven through the reverse osmosis membrane array by the high pressure, producing high salt concentration brine on the pressured side and fresh water on the low-pressure side at the end of the array. The high-pressure brine passes through an energy recovery device, such as a pressure exchanger or turbine, to recover the useful energy in the brine before it exits the system. These systems can be used to desalinate seawater or brackish water. Details of the individual system components are provided below.

7.3.1 Pretreatment

Pretreatment of the saline water is an essential step for reverse osmosis systems. Pretreatment methods are often custom designed for the specific characteristics of the raw water. Common methods employed for pretreatment in small PVRO systems start with simple filters which remove particulates from the incoming water. Usually these consist of two stages of filters to remove particles larger than 5 μm. Carbon filters are also commonly used to remove free chlorine from the incoming water. If the feedwater has high levels of bacteria, ozonation or chlorination are used to protect the reverse osmosis membranes from biofouling.[169]

Mineral scaling can also reduce the life of reverse osmosis membranes. This is particularly an issue for brackish water reverse osmosis systems where the recovery ratios tend to be higher. Methods of mitigating scale formation include the addition of antiscalants and decreasing the recovery ratio of the PVRO system.[170]

7.3.2 Pumps

Positive displacement pumps are commonly used for PVRO systems. Many systems in the literature use rotary positive displacement pumps such as vane pumps[171–173] or progressive cavity pumps.[174,175] Reciprocating pumps such as diaphragm pumps[176,177] or piston pumps[170,174] are also commonly used. The type of pump is chosen based on the flow rates

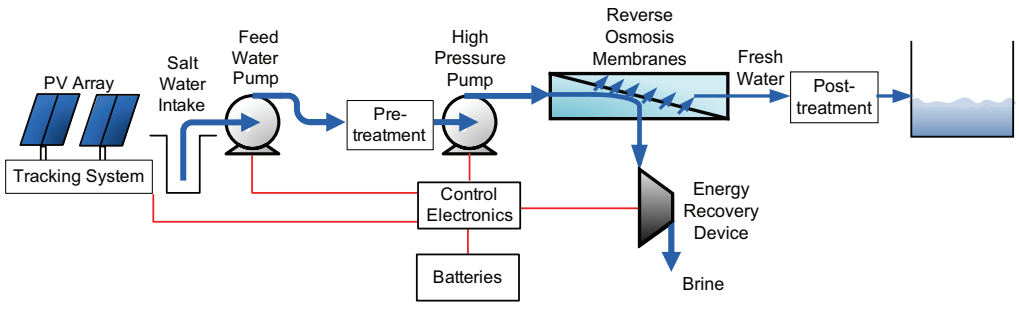

FIG. 30: PVRO system with energy recovery.

and pressures of the particular reverse osmosis system. Typical operating pressures for seawater reverse osmosis systems are between 55 and 70 bar. The typical operating pressures for a brackish water reverse osmosis system are usually substantially less, between 15 and 30 bar.

7.3.3 Reverse Osmosis Membranes

The reverse osmosis membranes are the essential component affecting separation. The prevalent construction used in PVRO systems are composite, spiral-wound membranes. The membrane itself is composed of a thin, nonporous polyamide active layer supported by a thicker, porous polysulfone backing. The membrane is configured as a cross-flow separator wherein a portion of the water is recovered. The rest leaves the membrane module as high concentrate brine.

The flow rate of clean water across the membrane is proportional to pressure difference minus the osmotic pressure difference, given by

$$\dot{V}_p = K_A A_{mem}\,(\text{TCF})\,(\text{FF})\left(\Delta\overline{P} - \Delta\overline{\pi}\right) \tag{7.3}$$

where A_{mem} is the membrane surface area, K_A is the membrane permeability for water, TCF is the water permeability temperature correction factor, FF is the membrane fouling factor, $\Delta\overline{P}$ is the average pressure applied across the membrane, and $\Delta\overline{\pi}$ is the average osmotic pressure applied across the membrane. This equation shows that increasing the membrane area, permeability, and driving pressure result in increased water production.

Unfortunately, the membranes are not perfect and also allow salt to be transmitted. The concentration of salts in the water produced is given by Ref. 178

$$C_p = \frac{K_B A_{mem}\,(pf)\,(\text{TCF})C_{fc}}{\dot{V}_p} \tag{7.4}$$

where K_B is the membrane permeability for salt, *pf* is the polarization factor, and C_{fc} is the average concentration of water in the membrane feed channel. This equation shows that the membrane area and salt permeability both affect the permeate concentration. These factors must be considered during the design process.

As can be seen in the equations above, the water flow rate through the reverse osmosis membrane is dependent on the driving pressure. Note the temperature correction factor: an increase in feedwater temperature of 4 degrees Kelvin will cause the product flow rate to increase by approximately 10% assuming that all other variables remain constant.[178] These effects should be considered when designing a PVRO system for a particular location.

7.3.4 Energy Recovery Devices

The brine exits the reverse osmosis module at high pressure. Energy from the high-pressure brine can be harnessed to perform useful work by introducing an energy recovery device. These devices can substantially reduce the power requirements for the reverse osmosis

process. This difference is shown in the energy flow diagrams. Figure 31 shows the energy flows in a reverse osmosis system without energy recovery. In this system, the majority of energy is lost in the pressure control valve that reduced the brine pressure to discharge pressure; the calculated specific energy consumption for this system is 9.8 kWh/m^3 of water produced. Figure 32 shows the energy flows in a system with a pressure exchanger energy recovery unit. In this case, less energy is required per unit of water produced: the calculated specific energy consumption is 3.8 kWh/m^3.

Energy recovery devices can greatly reduce the power requirements of a reverse osmosis system, but the available energy recovery options for small-scale PVRO systems are limited and tend to be expensive. As a result, many seawater PVRO systems have not incorporated energy recovery devices. Recently, energy recovery devices that can operate at lower flow rates have been developed. Devices that are incorporated in modern PVRO systems include Clark pumps, pressure exchangers, and hydraulic motors. Due to the lower pressure requirements and higher recovery rates, only a few brackish water reverse osmosis systems have incorporated pressure exchanger energy recovery devices.

7.3.5 Control Strategies and Batteries

Batteries are often a requirement in PV systems to store energy for times when the sun is not shining. However, in a PVRO system, we can store the energy in the form of clean water, eliminating the need for batteries. Therefore, including batteries in a PVRO system is a choice of the system designer. This section provides an overview of the pros and cons of including batteries in a PVRO system and control strategies that can be employed for PVRO systems.

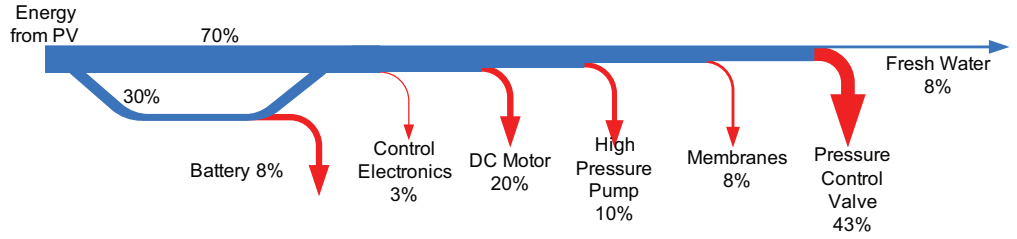

FIG. 31: Energy flows in reverse osmosis system without energy recovery.

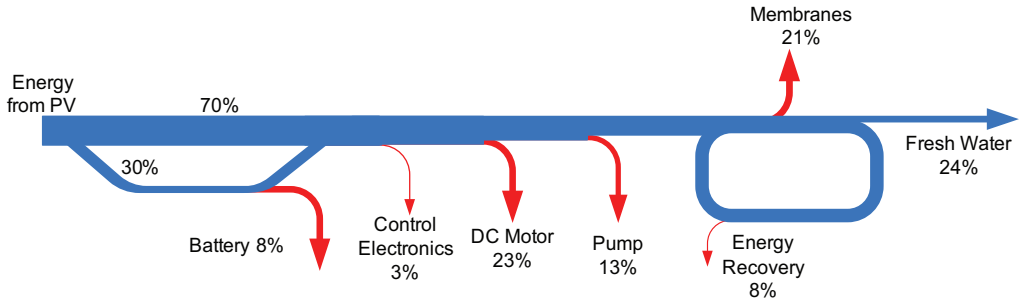

FIG. 32: Energy flows in reverse osmosis system with energy recovery.

Pros and Cons of Batteries: Batteries are included in a PVRO system for many reasons. Batteries can greatly simplify the operation of a system. Batteries allow for operation of the system at a constant set point. In addition, batteries can be used as a buffer to smooth out power variations over the course of the day and to operate during the nighttime hours.

Steady operation is believed to limit membrane biofouling. Researchers suggest that variable and intermittent operation can increase the rate at which biofouling occurs.[174,179−181] This is a particular concern for the hot climates where PVRO systems are typically deployed. However, the majority of biofouling research has been conducted for membranes at a fixed operating point. Studies have shown that the degradation of membranes under variable and intermittent operation is not a major concern over the short term,[175,179,182] but studies that quantify the long-term effects have yet to be completed. These long-term degradation effects should be factored into design decisions.

Despite simplifying system operation, the use of batteries has substantial drawbacks. First, batteries are expensive; installation and replacement costs of batteries significantly increase the lifetime cost of a PVRO system. Second, batteries require periodic maintenance. The absence of maintenance may result in greatly reduced battery life. Third, when charge controllers and wiring are considered, batteries result in a much more complicated PVRO system. Finally, batteries introduce energy conversion losses. Energy is lost when the electrical energy from the PV is converted to chemical energy in the battery and when the chemical energy is converted back to electrical energy to drive the pumps. These losses, shown in the energy flow diagrams (Figs. 31 and 32), decrease the overall system efficiency.

System Control Techniques: When using batteries, the control scheme for a PVRO system is simplified. Typical operation of a PVRO battery system is shown in Fig. 33. In these systems, the panel set point is controlled to maximize the power transferred to the batteries, the RO system is operated at a fixed point, and a simple controller determines the start-up and shutdown time.

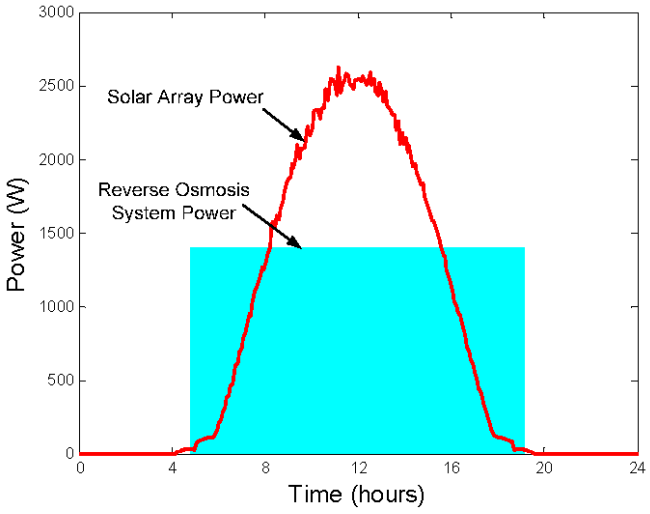

FIG. 33: Typical operation of a PVRO battery system.

Different techniques have been employed to determine the start-up and shutdown time of the battery-operated system. A simple technique checks the charge of the battery at sunrise and calculates a start-up time. At noon, the status of the batteries is measured and a shutdown time is determined.[183] Other simple approaches use a set battery voltage to trigger the system to turn on, and then use another battery voltage set point to turn the system off.[183,184] More complex dynamic regulation strategies have also been developed which delay the shutdown of the reverse osmosis system to ensure that frequent start-ups and shutdowns do not occur.[183]

System control without batteries becomes more complex. In this case, the system must respond to changes in environmental conditions such as solar radiation, water salinity, and temperature in real time. Without energy storage, this becomes a power management problem in which the controller varies the operating point of the pumps and other actuators in the reverse osmosis system. This type of control has been an active research area, and methods have been developed to optimize the PVRO system output under variable sunlight conditions.[173,178,183,185–187] When using one pump, one method optimizes system performance by controlling the operating power of the reverse osmosis pump to correspond to the maximum the PV panel power output.[186] In other methods, optimal operating points for the multiple pumps are determined offline and the controller tracks these points as the available solar power changes.[178,187] As noted above, biofouling is a concern, especially for variable operating systems without batteries. As a result, protocols are often implemented for battery-less PVRO systems that shut down the main reverse osmosis pumps and initiate flushing cycles during levels of low solar radiation.[173,183,185]

Thermal Control Techniques: It was shown in Sec. 7.2.2 that PV modules operate more efficiently when their temperature is lower. It was also shown in Sec. 7.3.3 that reverse osmosis membranes transmit more water when the input feedwater is warm. Techniques are currently being studied which exploit these complementary properties for a PVRO system.

In one approach, the reverse osmosis feedwater is run through a heat exchanger, which is affixed to the rear side of the PV panel.[188] This has the dual effect of cooling the PV, allowing it to produce more electricity, and warming the reverse osmosis feedwater, reducing the overall energy requirements of the reverse osmosis system. Furthermore, this approach allows for the addition of low-cost solar concentrators, which further boost the output of the reverse osmosis system. Careful control is required to ensure that the temperature limits of the PV and the RO are not exceeded. This approach has been shown to increase the overall performance of a PVRO system by 50%.

7.3.6 Overview of Deployed PVRO Systems

Many PVRO systems have been built and field tested. All of these systems are community scale, producing between 100 L and 60 m^3 of water per day. These systems can be divided into two main categories: brackish water systems and seawater systems.

Brackish water PVRO systems have been designed and tested in a wide range of locations.[170–173,175,176,189–197] Many of these systems are simple and do not incorporate an energy recovery device due to the small scale and reduced pressure requirements

for brackish water PVRO systems. Examples include a small system designed by Carvalho and Riffel in Brazil,[197] a system designed and tested by Cheah in the Southwestern United States,[173] a small system was tested by Abdallah in Jordan,[194] and a small system tested by Joyce in Portugal.[175] Some small brackish water PVRO systems incorporate energy recovery devices. The most notable of these systems is SolarFlow, which has been tested in the Outback of Australia.[196] Some characteristics of these systems and estimated water costs are presented in Table 8.

Seawater PVRO systems have also been developed.[174,177,179,183,185,198−201] Many of the early systems were simply a photovoltaic array and battery bank used to power an existing reverse osmosis system. Such systems were found to be inefficient, so recent research has focused on increasing system efficiency, with some success. The Canary Islands Technological Institute has developed a small battery-based system.[183,198] Battery-based systems have also been commercialized by Spectra Watermakers.[201] In addition, hybrid solar/wind reverse osmosis systems have been developed.[181,185,199] Re-

TABLE 8: A selection of brackish water PVRO systems

Location	Water salinity (mg/L)	Water production (m^3/day)	PV power rating (kW_p)	Batteries (kWh)	Energy recovery	Water cost ($US/$m^3$)	Year
Amman, Jordan[194]	400	0.1	0.07	No	No	N/A	2005
Cituis, Indonesia[189]	3500	12.0	25.7	132	No	$3.68	1983
Coité–Pedreiras, Brazil[192]	1200	0.55	1.1	9.6	No	$12.76	2004
Concepcion del Oro, Mexico[190]	3000	0.71	2.5	No	No	N/A	1978
El-Mamrawein, Egypt[193]	5000	53.0	18.5	200	No	N/A	1986
Gillen Bore, Australia[170]	1600	1.2	0.52	Yes	No	N/A	1993
Giza, Egypt[193]	BW	6.0	7.0	Yes	No	N/A	1980
Hammam Lif, Tunisia[195]	2800	0.05	0.59	No	No	$8.00	2005
Heelat Ar Rakah, Oman[171,191]	1010	5.0	3.4	9.6	No	$6.52	1998
Lisbon, Portugal[176]	2549	0.02	0.1	No	No	N/A	2000
Mesquite, Nevada[173]	3910	1.5	0.54	No	No	$3.46	2003
Perth, Australia[170]	BW	0.55	1.2	Yes	No	N/A	1982
Pine Hill, Australia[175]	5,300	1.1	0.6	No	Yes	N/A	2008
Sadous, Saudi Arabia[190]	5700	5.7	10.1	264	No	N/A	1994
White Cliffs, Australia[172]	3500	0.5	0.34	No	Yes	N/A	2003

search has also led to the development of cost-effective seawater PVRO systems without batteries.[174,177,179,183,198,200] Some characteristics of these seawater PVRO systems and estimated water costs are presented in Table 9.

Cost analyses of PVRO systems have been performed by multiple researchers. The results of these analyses are summarized in Tables 8 and 9. Reported numbers range between \$3.00 per m^3 and \$12.76 per m^3. These numbers will vary greatly for different locations due to the variation in solar resource. There have been dramatic decreases in the cost of PV panels in the past few years, which should make PVRO systems more cost competitive.

7.4 PVED Systems

7.4.1 System Overview

Electrodialysis (ED) is an electrochemical process that can be used to desalinate water. Due to the energy requirements of the process, electrodialysis is much more cost effective for lower salinity water, and it is typically implemented for purification only with brackish water sources. The typical PVED system can be seen in Fig. 34, consisting of a PV panel array, control electronics, a battery, a feed pump, an electrodialysis membrane stack, and pre- and post-treatment systems.

The principle of the electrodialysis process is shown in Fig. 35. In this process, the salt is separated from the water based on an electric charge. In this system, two conductive electrodes are connected to a voltage source and are placed in contact with the brackish

TABLE 9: A selection of seawater PVRO systems

Location	Water salinity (mg/L)	Water production (m^3/day)	PV power rating (kW_p)	Batteries (kWh)	Energy recovery	Water cost (\$US/m^3)	Year
Athens, Greece[200]	40,000	0.35	0.85	No	Yes	\$11.45	2008
Boston, MA[177]	35,000	0.4	0.23	No	Yes	N/A	2010
Canary Islands, Spain [183,198]	35,500	3.0	4.8	60	Yes	\$9.60	1998
Massawa, Eritia[174,179]	32,800	3.0	2.4	No	Yes	\$3.00	2001

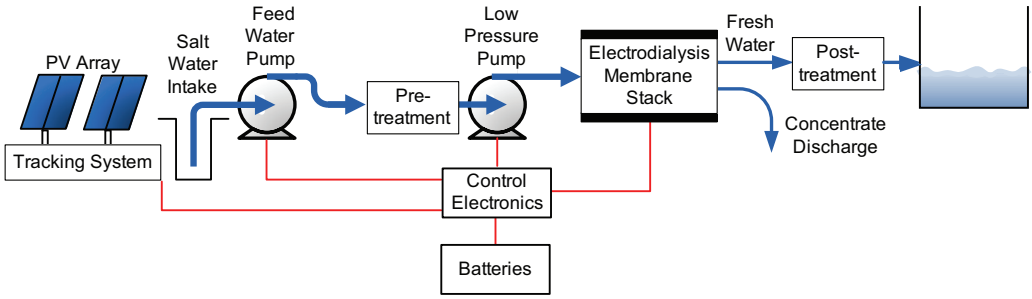

FIG. 34: Typical operation of a PVRO battery system.

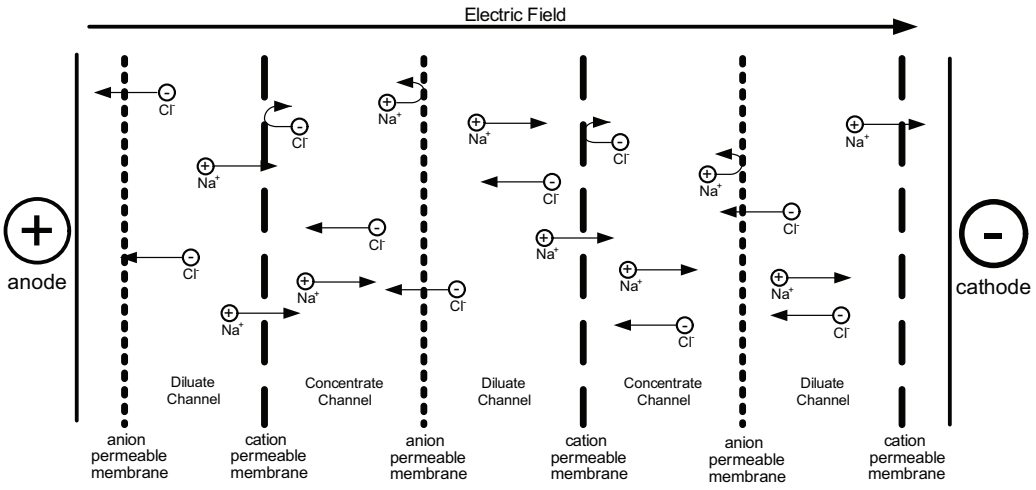

FIG. 35: Typical operation of a PVRO battery system.

water. An electric field is established and charged ions migrate toward the electrode with the opposite charge. Two types of selectively permeable membranes are placed between the two electrodes. An anion exchange membrane is positively charged and only allows transmission of negative ions (anions), while a cation exchange membrane is negatively charged and only allows transmission of positive ions (cations). These membranes are stacked in an alternating fashion, as shown in Fig. 35, resulting in alternating channels of diluate and concentrate which can easily be collected.

7.4.2 Deployed PVED Systems

Photovoltaic electrodialysis systems have been successfully constructed and tested in the field. The majority of these systems use batteries to provide a constant power source. Laboratory scale systems include systems built at the University of Bahrain.[202] Systems have also been field tested at the University of Alicante in Spain,[203] at Fukue City in Japan,[204] at Rajasthan in India,[205] and at the Bureau of Reclamation in New Mexico.[206] Details of these systems are given in Table 10.

TABLE 10: Summary of deployed PVED systems

Location	**Water salinity (mg/L)**	**Water production (m^3/day)**	**PV power rating (kW_p)**	**Batteries**	**Water cost ($US/$m^3$)**	**Year**
Alicante, Spain[203]	5100	15	3.8	No	N/A	2008
Fukue City, Japan[204]	1000	200	N/A	Yes	N/A	1994
Rajasthan, India[205]	5000	1 .0	0.45	Yes	$5.80	1986
Spencer Valley, New Mexico[206]	1000	2.8	3.3	Yes	$16.00	1998

Cost analyses of PVED systems have been performed by multiple researchers. The results of these analyses are overviewed in Table 10. Reported numbers range between \$5.80 per m^3 and 16.00 per m^3. Note that these cost numbers were reported prior to 1998. Since then, there has been a dramatic decrease in the cost of PV panels, which should make PVED systems more cost competitive.

7.5 Summary Comments on PV Powered Desalination

This section provided an overview of different PV powered desalination options. The fundamentals of photovoltaic system technology were discussed, and the properties of PVRO and PVED systems were presented. This section also summarized PVRO and PVED systems that have been built and tested under field conditions. Cost analysis for the deployed PVRO systems show water cost ranges between \$3.00 per m^3 and \$13.00 per m^3. Reported cost numbers for PVED systems range between \$5.80 per m^3 and \$16.00 per m^3. These prices are high when compared to large-scale desalination plants, but with decreases in the costs of PV materials and improvements in system technologies, these systems are expected to become more financially viable.

8. FINAL COMMENTS

Solar desalination is attractive as a renewably powered means of providing fresh water at both large and small scales, and many of the world's water-scarce regions have abundant solar energy. This review has considered basic concepts of desalination, simple solar stills, solar-driven humidification–dehumidification systems, solar-driven membrane distillation, concentrated-solar-driven combined water-power coproduction, and photovoltaic-driven desalination. While solar stills are a relatively well-established and low-efficiency technology, most of the other, higher efficiency systems are the targets of considerable ongoing research and development, and the cost of water from each is dropping rapidly. Some of these technologies (HDH, MD, PV) are probably best suited for smaller scale or off-the-grid applications, but the concentrated solar distillation technologies show considerable potential for large-scale water production, with estimated costs well below 1 €/m^3. Many water-stressed regions are also rapidly developing substantial solar power generation capacity, and it is clear that for those regions solar electrical generation will be a major driver for the development of solar desalination technologies. It can be predicted that solar-driven desalination will have a significant role in supplying the world's fresh water in the years to come.

ACKNOWLEDGMENTS

The first and third author acknowledge support from King Fahd University of Petroleum and Minerals through the Center for Clean Water and Clean Energy at MIT and KFUPM. The second author acknowledges support provided by NSTIP unit at KFUPM under project number 08-WAT79-4. The fourth and fifth authors acknowledge the support provided by the Spanish Ministry of Economy and Competitiveness and SolarPACES.

REFERENCES

1. UNEP/GRID-Arendal. Water Scarcity Index [Internet], UNEP/GRID-Arendal Maps and Graphics Library; 2009, Retrieved July 24, 2011, from http://maps.grida.no/go/graphic/water-scarcity-index.
2. V. Smakhtin, C. Revenga, and P. Döll, Taking into Account Environmental Water Requirements in Global-scale Water Resources Assessments, Comprehensive Assessment Research Report 2, Comprehensive Assessment Secretariat, International Water Management Institute, Colombo, 2004.
3. T. Oki and S. Kanae, Global hydrological cycles and world water resources, *Science*, **313**:1068–1072, 2006.
4. J. Kucera, ed., *Desalination: Water from Water, Scrivener*, Scrivener Publishing LLC, Salem, MA, in preparation.
5. UNESCO, The Practical Salinity Scale 1978 and the International Equation of State of Seawater 1980, Technical Paper Mar. Sci., vol. 36, 1981.
6. K. S. Spielger and Y. M. El Sayed, *A Desalination Primer*, Balaban Desalination Publications, L'Aquila, Italy, 1994.
7. R. Stewart, *Introduction to Physical Oceanography*, Chap. 6, Texas A&M University, College Station, TX, 2007.
8. World Health Organization, *Desalination for Safe Water Supply*, World Health Organization, Geneva, 2007.
9. M. Wilf, *The Guidebook to Membrane Desalination Technology*, Appendix A, Balaban Desalination Publications, L'Aquila, Italy, 2007.
10. Massachusetts Water Resources Authority, Water Quality Update, Boston, July and Dec. 2007.
11. World Health Organization, *Guidelines for Drinking-Water Quality*, 3rd ed., vol. 1, World Health Organization, Geneva, 2004.
12. United States Environmental Protection Agency, *National Primary Drinking Water Regulations*, National Secondary Drinking Water Regulations.
13. M. H. Sharqawy, J. H. Lienhard V, and S. M. Zubair, The thermophysical properties of seawater: A review of existing correlations and data, *Desalination Water Treatment*, **16**:354–380, 2010.
14. M. H. Sharqawy, J. H. Lienhard V, and S. M. Zubair, On exergy calculations for seawater with application to desalination systems, *Int. J. Thermal Sci.*, **50**(2):187–196, 2011.
15. International Association for the Properties of Water and Steam, Release on the IAPWS formulation for the thermodynamic properties of seawater, available at www.iapws.org, 2008.
16. V. Belessiotis, E. Delyannis, and M. Balaban, *The ABC of Solar Desalination*, Balaban Desalination Publications, L'Aquila, Italy, in preparation.
17. F. Rahman and Z. Amjad, Scale formation and control in thermal desalination systems, in *The Science and Technology of Industrial Water Treatment*, Chap. 14, CRC Press, Boca Raton, 2010.
18. International Desalination Association, *IDA Desalination Yearbook 2010–2011*, Media Analytics LTD, Oxford, United Kingdom, 2010.

19. FAO, Total water use data from 1998–2002, FAO of the UN, Data from Aquastat, 2010.
20. J. F. Kenny, N. L. Barber, S. S. Hutson, K. S. Linsey, J. K. Lovelace, and M. A. Maupin, Estimated Water Use in the United States in 2005, USGS Circular 1344, United States Geological Survey, Reston, VA, 2009.
21. K. H. Mistry, R. K. McGovern, G. P. Thiel, E. K. Summers, S. M. Zubair, and J. H. Lienhard V, Entropy generation analysis of desalination technologies, *Entropy*, **13**(10):1829–1864, 2011.
22. G. P. Narayan, R. K. McGovern, J. H. Lienhard V, and S. M. Zubair, Variable pressure humidification dehumidification desalination systems, in *Proc. 8th ASME/JSME Thermal Engineering Joint Conf.*, Honolulu, March 2011.
23. Y. M. El-Sayed and R. S. Silver, Fundamentals of Distillation, in *Fundamentals of Desalination,* 2nd ed., K. S. Spielger and A. D. K. Laird, eds., vol. A, Academic Press, New York, pp. 55–109, 1980.
24. K. H. Mistry, J. H. Lienhard V, and S. M. Zubair, Effect of entropy generation on the performance of humidification-dehumidification desalination cycles, *Int. J. Thermal Sci.*, **49**(9):1837–1847, 2010.
25. R. Borsani, MSF System: Present status and future direction, Desalination: An energy solution, in *Intl. Desalination Association Conf.*, Huntington Beach, CA, Nov. 2–3, 2010.
26. C. Temster and J. Laborie, Dual purpose desalination plant—high efficiency multi-effect evaporator operating with turbine for power production, in *Proc. IDA World Conf. on Desalination and Water Science*, Abu Dhabi, **3**:297–308, 1995.
27. C. Desportes, MED Industrial System: Present status and future directions, Desalination: An energy solution, in *Intl. Desalination Association Conf.*, Huntington Beach, CA, Nov. 2–3, 2010.
28. G. Crisp, Actual energy consumption and water cost to the SWRO systems at Perth, Desalination: An energy solution, in *Intl. Desalination Association Conf.*, Huntington, Beach, CA, Nov. 2–3, 2010.
29. G. Crisp, personal communication to J. H. Lienhard V, July 2011.
30. R. Balan, J. Chandrasekaran, S. Shanmugan, B. Janarthanan, and S. Kumar, Review on passive solar distillation, *Desalination Water Treatment*, **28**:217–218, 2011.
31. A. I. Kudish, E. G. Evseev, G. Walter, and T. Priebe, Simulation study on a solar desalination system utilizing an evaporator/condenser chamber, *Energy Convers. Manage.*, **44**(10):1653–1670, 2003.
32. B. W. Tleimat and E. D. Howe, Nocturnal production of solar distiller, *Solar Energy*, **10**(2):61–66, 1966.
33. B. W. Tleimat and E. D. Howe, Comparison of plastic and glass condensing covers for solar distillers, *Solar Energy*, **12**(3):293–296, 1969.
34. M. A. Antar and S. M Zubair, Performance evaluation of a solar still in the Eastern Province of Saudi Arabia—An improved analysis, *Desalination Water Treatment*, **22**:100–110, 2010.
35. J. A. Clark, The steady-state performance of a solar still, *Solar Energy*, **44**(1):43–49, 1990.
36. G. N. Tiwari, A. Kupfermann, and A. Agrawal, A new design of double condensing chamber solar still, *Desalination*, **114**(2):153–164, 1997.
37. T. Kiatsiriroat, Review of research and development on vertical solar stills, *ASEAN J. Sci.*

Technol. Dev., **6**(1):15, 1989.

38. B. I. Ismail, Design and performance of a transportable hemispherical solar still, *Renewable Energy*, **34**(1):145–150, 2009.
39. S. Suneja and G. N. Tiwari, Optimization of number of effects for higher yield from an inverted absorber solar still using the Runge–Kutta method, *Desalination*, **120**(3):197–209, 1999.
40. H. Tanaka, T. Nosoko, and T. Nagata, Parametric investigation of a basin-type-multiple-effect coupled solar still, *Desalination*, **130**(3):295–304, 2000.
41. H. Tanaka, T. Nosoko, and T. Nagata, A highly productive basin type multiple-effect coupled solar still, *Desalination*, **130**(3):279–293, 2000.
42. M. I. Ahmed, M. Hrairi, and A. F. Ismail, On the characteristics of multistage evacuated solar distillation, *Renewable Energy*, **34**:1471–1478, 2009.
43. E. Delyannis, Historic background of desalination and renewable energies, *Solar Energy*, **75**(5):357–366, 2003.
44. H. Al-Hinai, M. S. Al-Nassri, and B. A. Jubran, Parametric investigation of a double effect solar still in comparison with a single effect solar still, *Desalination*, **150**:75–83, 2002.
45. H. Tanaka, Y. Nakatake, and M. Tanaka, Indoor experiments of the vertical multiple-effect diffusion-type solar still coupled with a heat-pipe solar collector, *Desalination*, **177**:291–302, 2005.
46. A. A. Al-Karaghouli and W. E. Alnaser, Experimental comparative study of the performances of single and double basin solar stills, *Appl. Energy*, **77**(3):317–325, 2004.
47. A. A. Al-Karaghouli and W. E. Alnaser, Performances of single and double basin solar-stills. *Appl. Energy*, **8**(3):347–354, 2004.
48. B. A. Jubran, M. I. Ahmed, A. F. Ismail, and Y. A. Abakar, Numerical modeling of a multi-stage solar still, *Energy Convers. Manage.*, **41**:1107–1121, 2000.
49. P. C. Lobo and S. R Araujo, A simple multi-effect basin type solar still, SUN, in *Proc. of Intl. Solar Energy Society*, vol. 3, Pergamon Press, Oxford, pp. 2026–2030, 1978.
50. A. K. Abu Hijleh and H. M. Rababa'h, Experimental study of a solar still with sponge cubes in basin, *Energy Convers. Manage.*, **44**:1411–1418, 2003.
51. G. N. Tiwari, Demonstration plant of multi-wick solar still, *Energy Convers. Manage.*, **24**(4):313–316, 1984.
52. M. M. Naim and M. A. Abd El-Kawi, Non-conventional solar stills, Part 1. Non-conventional solar stills with charcoal particles as absorber medium, *Desalination*, **153**:55–64, 2002.
53. V. A. Akinsete and C. U. Duru, A cheap method of improving the performance of roof type solar stills, *Solar Energy*, **23**(3):271–272, 1979.
54. S. Nijmeh, S. Odeh, and B. Akash, Experimental and theoretical study of a single-basin solar still in Jordan, *Int. Commun. Heat Mass Transfer*, **32**:565–572, 2005.
55. M. M. Naim and M. A. Abd El-Kawi, Non-conventional solar stills, Part 2: Non-conventional solar stills with energy storage element, *Desalination*, **153**:71–80, 2002.
56. M. F. A Goosen, S. S. Sablani, W. H Shayya, C. Paton, and H. Al-Hinai, Thermodynamic and economic considerations in solar desalination, *Desalination*, **129**:63–89, 2000.
57. Z. S. Abdel-Rehim and A. Lasheen, Experimental and theoretical study of a solar desalination system located in Cairo, Egypt, *Desalination*, **217**:52–64, 2007.

58. N. Hussain and A. Rahim, Utilization of new technique to improve the efficiency of horizontal solar desalination still, *Desalination*, **138**:121–128, 2001.
59. A. El-Bahi and D. Inan, A solar still with minimum inclination, coupling to an outside condenser, *Desalination*, **123**:79–83, 1999.
60. B. Bouchekima, B. Gros, R. Ouahes, and M. Diboun, Brackish water desalination with heat recovery, *Desalination*, **138**:147–155, 2001.
61. M. T. Chaibi, Analysis by simulation of a solar still integrated in a greenhouse roof, *Desalination*, **128**:123–138, 2000.
62. M. Radhwan and H. E. S. Fath, Thermal performance of greenhouses with a built-in solar distillation system: Experimental study, *Desalination*, **181**:193–205, 2005.
63. E. G. Marí, R. P. G. Colomer, and C. A. Blaise-Ombrecht, Performance analysis of a solar still integrated in a greenhouse, *Desalination*, **203**:435–443, 2007.
64. S. Kumar and G. N. Tiwari, Optimization of collector and basin areas for a higher yield active solar still, *Desalination*, **116**:1–9, 1998.
65. K. Voropoulos, E. Mathioulakis, and V. Belessiotis, Experimental investigation of a solar still coupled with solar collectors, *Desalination*, **138**:103–110, 2001.
66. S. Satcunanathan and H. P. Hanses, An investigation of some of the parameters involved in solar distillation, *Solar Energy*, **14**:353–363, 1973.
67. V. B. Sharma and S. C. Mullick, Calculations of hourly input of a solar still, *J. Solar Energy Eng.*, **115**:231–236, 1993.
68. V. B. Sharma and S. C. Mullick, Estimation of heat transfer coefficients, the upward heat flow, and evaporation in a solar still, *ASME J. Solar Energy Eng.*, **113**:36–41, 1991.
69. P. I. Cooper, The maximum efficiency of single effect solar stills, *Solar Energy*, **15**:205–217, 1973.
70. M. Mimaki, K. Tanaka, and K. Watanabe, The performance of solar stills, *Energy Dev. Japan*, **3**:207–225, 1981.
71. Y. P. Yadaf and Y. N. Prasad, Parametric investigation of a basing type solar still, *Energy Convers. Manage.*, **31**:7–16, 1991.
72. Y. P. Yadav and B. P. Yadav, Transient analytical solution of a solar still integrated with a tubular solar energy collector, *Energy Convers. Manage.*, **39**(9):927–930, 1998.
73. M. K. Phadatare and S. K. Verma, Effect of cover materials on heat and mass transfer coefficients in a plastic solar still, *Desalination Water Treatment*, **2**:248–253, 2009.
74. N. Khalifa and A. M. Hamood, Experimental validation and enhancement of some solar still performance correlations, *Desalination Water Treatment*, **4**:311–315, 2009.
75. G. M. Cappelletti, An experiment with a plastic solar still, *Desalination*, **142**:221–227, 2002.
76. H. Al-Hinai, M. S. Al-Nassri, and B. A. Jubran, Effect of climatic, design and operational parameters on the yield of a simple solar still, *Energy Convers. Manage.*, **43**:1639–1650, 2002.
77. J. A. Duffie and W. A. Beckman, *Solar Engineering of Thermal Processes*, 3rd ed., John Wiley and Sons, Hoboken, NJ, 2006.
78. R. V. Dunkle, Solar water distillation: The roof type still and a multiple effect diffusion still, *International Developments In Heat Transfer*, New York, ASME. Part V, pp. 895–902, 1961. Papers presented at the Intl. Heat Transfer Conf., University of Colorado, Boulder, Aug. 28–

Sept. 1, 1961.

79. G. N. Tiwari, S. K. Shukla, and I. P. Singh, Computer modeling of passive/active solar stills by using inner glass temperature, *Desalination*, **154**:171–185, 2003.
80. R. Tripathi and G. N. Tiwari, Thermal modeling of passive and active solar stills for different depths of water by using the concept of solar fraction, *Solar Energy*, **80**:956–967, 2006.
81. K. G. T. Hollands, T. E. Unny, G. D. Raithby, and L. Konicek, Free convection heat transfer across inclined air layers, *J. Heat Transfer*, **98**:189, 1976.
82. E. M. J. Sparrow, J. W. Ramsey, and E. A. Mass, Effect of finite width on heat transfer and fluid flow about an inclined rectangular plate, *J. Heat Transfer*, **101**:2, 1979.
83. G. N. Tiwari and H. N. Singh, Solar Distillation, *in Encyclopedia of Life Support Systems*, vol. II., Solar Energy Conversion and Photoenergy Systems, Developed under the Auspices of the UNESCO, Eolss Publishers, Oxford, UK, 2004.
84. G. P. Narayan, M. H. El-Sharqawy, E. K. Summers, J. H. Lienhard, S. M. Zubair, and M. A Antar, The potential of solar-driven humidification-dehumidification desalination for small-scale decentralized water production, *Renewable Sustainable Energy Rev.*, **14**(4):1187–1847, 2010.
85. S. Al-Hallaj, M. M. Farid, and A. R. Tamimi, Solar desalination with a humidification dehumidification cycle: Performance of the unit, *Desalination*, **120**(3):273–280, 1998.
86. H. Muller-Holst, M. Engelhardt, and W. Scholkopf, Small-scale thermal seawater desalination simulation and optimization of system design, *Desalination*, **122**:255–262, 1999.
87. S. Al-Hallaj and J. R. Selman, A comprehensive study of solar desalination with a humidification-dehumidification cycle, Middle East Desalination Research Center Report 98–BS–032b, 2002.
88. Y. J. Dai, R. Z. Wang, and H. F. Zhang, Parametric analysis to improve the performance of a solar desalination unit with humidification and dehumidification, *Desalination*, **142**:107–118, 2002.
89. J. Orfi, M. Laplante, H. Marmouch, N. Galanis, B. Benhamou, S. Ben Nasrallah, and C. T. Nguyen, Experimental and theoretical study of a humidification-dehumidification water desalination system using solar energy, *Desalination*, **168**:151–159, 2010.
90. H. Shaobo, Y. Shengquan, and H. Zhang, Performance optimization of solar humidification-dehumidification desalination process using pinch technology, *Desalination*, **183**(1–3):143–149, 2005.
91. E. Chafik, A new water desalination process using solar energy, *Desalination*, **153**:25–37, 2002.
92. E. Chafik, A new type of seawater desalination plants using solar energy, *Desalination*, **156**:333–348, 2003.
93. E. Chafik, Design of plants for solar desalination using the multi-stage heating/humidifying technique, *Desalination*, **168**:55–71, 2004.
94. H. E. S. Fath and A. Ghazy, Solar desalination using humidification-dehumidification technology, *Desalination*, **142**:119–133, 2002.
95. C. Yamali and I. Solmus, Theoretical investigation of a humidification dehumidification desalination system configured by a double-pass flat plate solar air heater, *Desalination*, **205**:163–177, 2007.

96. C. Yamali and I. Solmus, Theoretical investigation of a humidification dehumidification desalination system configured by a double-pass flat plate solar air heater, *Desalination*, **220**(1–3):538–551, 2008.

97. A. S. Nafey, H. E. F. Fath, S. O. El-Helaby, and A. M. Soliman, Solar desalination using humidification-dehumidification processes. Part I. A numerical investigation, *Energy Convers. Manage.*, **45**:1243–1261, 2004.

98. R. H. Xiong, S. C. Wang, L. X. Xie, Z. Wang, and P. L. Li, Experimental investigation of a baffled shell and tube desalination column using the humidification-dehumidification process, *Desalination,* **180**(1–3):253–261, 2005.

99. R. H. Xiong, S. C. Wang, L. X. Xie, Z. Wang, and P. L. Li, A mathematical model for a thermally coupled humidification–dehumidification desalination process, *Desalination* **196**:177–187, 2006.

100. S. Yanniotis and K. Xerodimas, Air humidification for seawater desalination, *Desalination*, **158**:313–319, 2003.

101. H. Ben-Basha, T. Damak, and M. Bouzguenda, Experimental validation of the distillation module of a desalination station using SMCEC principle, *Renewable Energy*, **28**:2335–2354, 2003.

102. M. M. Farid and A. W. Al-Hajaj, Solar desalination with humidification dehumidification cycle: Mathematical modeling of the unit, *Desalination*, **106**:427–429, 1996.

103. A. S. Nafey, H. E. S. Fath, S. O. El-Helaby, and A. M. Soliman, Solar desalination using humidification–dehumidification processes, Part II: An experimental investigation, *Energy Convers. Manage.*, **45**(7–8):1263–1277, 2004.

104. N. K. Nawayseh, M. M. Farid, S. Al-Hallaj, and A. R. Tamimi, Solar desalination based on humidification process. Part I. Evaluating the heat and mass transfer coefficients, *Energy Convers. Manage.*, **20**:1423–1439, 1992.

105. I. Houcine, M. B. Amara, A. Guizani, and M. Maalej, Pilot plant testing of a new solar desalination process by a multiple-effect-humidification technique, *Desalination*, **196**:105–124, 2006.

106. J. A. Duffie and W. A. Beckman, *Solar Energy Thermal Processes*, Wiley, New York, 1974.

107. I. A. Shabaneh, P. Gandhidasan, M. A. Antar, and H. Baig, Simulation of HDH desalination system using tilted, two-pass solar air heater, in *15th Intl. Water Technology Conf., IWTC 15*, May 28–30, Alexandria, Egypt, 2010.

108. G. P. Narayan, K. H. Mistry, M. H. Sharqawy, S. M. Zubair, and J. H. Lienhard V, Energy effectiveness of simultaneous heat and mass exchange devices, *Frontiers Heat Mass Transfer*, **1**(2):1–13, 2010.

109. M. F. A. Goosen, S. S. Sablani, W. H. Shayya, C. Paton, and H. Al-Hinai, Thermodynamic and economic considerations in solar desalination, *Desalination*, **129**:63–89, 2000.

110. M. Khedr, Techno-economic investigation of an air humidification-dehumidification desalination process, *Chem. Eng. Technol.*, **16**:270–274, 1993.

111. J. F. Klausner and R. Mei, Diffusion Driven Desalination Apparatus and Process, US Patent no. 6,919,000, 2005.

112. G. P. Narayan, M. H. El-Sharqawy, J. H. Lienhard V, and S. M. Zubair, Thermodynamic analysis of humidification-dehumidification desalination cycles, *Desalination Water Treatment*, **16**:339–353, 2010.

113. G. P. Narayan, J. H. Lienhard V, and S. M. Zubair, Entropy generation minimization of combined heat and mass exchange devices, *Int. J. Thermal Sci.*, **49**(10):2057–2066, 2010.

114. G. P. Narayan, J. H. Lienhard V, and S. M. Zubair, Entropy generation minimization of combined heat and mass transfer devices, *Int. J. Thermal Sci.*, **49**(10):2057–2066, 2010.

115. K. H. Mistry, J. H. Lienhard V, and S. M. Zubair, Effect of entropy generation on the performance of humidification-dehumidification desalination cycles, *Int. J. Thermal Sci.*, **49**(9):1837–1847, 2010.

116. M. H. El-Sharqawy, G. P. Narayan, J. H. Lienhard V, and S. M. Zubair, Water Separation under Reduced Pressure, Patent pending, USSN 12/554,726.

117. G. P. Narayan, M. H. El-Sharqawy, J. H. Lienhard V, and S. M. Zubair, Water Separation under Varied Pressure, Patent pending, USSN 12/573,221.

118. K. W. Lawson and D. R. Lloyd, Membrane distillation, *J. Membr. Sci*., **124**:1–25, 1997.

119. J. I. Mengual and L. Peña, Membrane distillation, *Colloid Interface Sci.*, **1**:17–29, 1997.

120. M. S. El-Bourawi, Z. Ding, R. Ma, and M. Khayet, A framework for better understanding membrane distillation separation process, *J. Membr. Sci.*, **285**:4–29, 2006.

121. J. P. Méricq, S. Laborie, and C. Cabassud, Vacuum membrane distillation of seawater reverse osmosis brines, *Water Res.*, **44**(18):5260–5273, 2010.

122. C. M. Tun, A. G. Fane, J. T. Matheickal, and R. Sheikholeslami, Membrane distillation crystallization of concentrated salts-flux and crystal formation, *J. Membr. Sci.*, **257**:144–155, 2005.

123. E. Drioli, A. Criscuoli, and E. Curcio, Integrated membrane operation for seawater desalination, *Desalination*, **147**: 77–81, 2002.

124. A. M. Alklaibi and N. Lior, Membrane-distillation desalination: Status and potential, *Desalination*, **171**:111–131, 2004.

125. A. M. Alklaibi and N. Lior, Heat and mass transfer resistance analysis of membrane distillation, *J. Membr. Sci.*, **285**:362–369, 2006.

126. T. Gullinkala, B. Digman, C. Gorey, R. Hausman, and I. C. Escobar, Desalination: Reverse Osmosis and Membrane Distillation, Chap. 4 in *Sustainability Science and Engineering*, C. E. Isabel and I. S. Andrea, eds., Elsevier, Amsterdam, vol. 2, pp. 65–93, 2010.

127. Z. Ding, L. Liu, M. S. El-Bourawi, and R. Ma, Analysis of a solar-powered membrane distillation system, *Desalination*, **172**:27–40, 2005.

128. P. A. Hogan, Sudjito, A. G. Fane, and G. L. Morrison, Desalination by solar heated membrane distillation, *Desalination*, **81**:81–90, 1991.

129. M. Banat, R. Jumah, and M. Garaibeh, Exploitation of solar energy collected by solar stills from desalination by membrane distillation, *Renewable Energy*, **25**:293–305, 2002.

130. C. Bier and U. Plantikow, Solar-powered desalination by membrane distillation (MD), in *IDA World Congress on Desalination and Water Sciences*, Abu Dhabi, Nov. 18–24, 1995; available at http://www2.hawaii.edu/∼nabil/solar.htm.

131. J. Koschikowski, M. Wieghaus, and M. Rommel, Solar thermal-driven desalination plants based on membrane distillation, *Desalination*, **156**:295–304, 2003.

132. F. Banat, N. Jwaied, M. Rommel, J. Koschikowski, and M. Wieghaus, Performance evaluation of the large SMADES autonomous desalination solar-driven membrane distillation plant in Aqaba, Jordan, *Desalination*, **217**:17–28, 2007.

133. F. Banat, N. Jwaied, M. Rommel, J. Koschikowski, and M. Wieghaus, Desalination by a compact SMADES autonomous solar-powered membrane distillation unit, *Desalination*, **217**:29–37, 2007.

134. J. Koschikowski, M. Wieghaus, M. Rommel, V. Subiela-Ortin, B. Peñate-Suarez, and J. R. Betancort-Rodríguez, Experimental investigations on solar driven stand-alone membrane distillation systems for remote areas, *Desalination*, **248**:125–131, 2009.

135. J. Walton, H. Lu, C. Turner, S. Solis, and H. Hein, Solar and Waste Heat Desalination by Membrane Distillation, Desalination and Water Purification Research and Development Program Report no. 81, U.S. Department of the Interior, Bureau of Reclamation, Denver, 2004.

136. J. Blanco-Galvez, L. Garcia-Rodriguez, and I. Martin-Mateos, Seawater desalination by an innovative solar-powered membrane distillation system: The MEDESOL project, *Desalination*, **246**:567–576, 2009.

137. E. Guillén-Burrieza, J. Blanco, G. Zaragoza, D.-C. Alarcón, P. Palenzuela, M. Ibarra, and W. Gernjak, Experimental analysis of an air gap membrane distillation solar desalination pilot system, *J. Membr. Sci.*, **379**(1–2):386–396, 2011.

138. A. E. Jansen, J. H. Hanemaaijer, J. van Medevoort, C. Dotremont, and E. van Sonsbeek, Memstill membrane distillation: A future desalination technology, in *Proc. of Intl. Conf. Advances in Science and Engineering for Brackish Water and Seawater Desalination*, Cetraro, Italy, ECI, May 8–12, pp. 82–84, 2010.

139. E. Guillén-Burrieza, S. Miralles, G. Zaragoza, and J. Blanco, Experimental evaluation of two pilot-scale membrane distillation modules used for solar desalination, *J. Membr. Sci.*, **409-410**:264–275, 2012.

140. C. Cabassud and D. Wirth, Membrane distillation for water desalination: How to choose an appropriate membrane?, *Desalination*, **157**:307–314, 2003.

141. X. Wang, L. Zhang, H. Yang, and H. Chen, Feasibility research of potable water production via solar-heated hollow fiber membrane distillation system, *Desalination*, **247**:403–411, 2009.

142. J. P. Mericq, S. Laborieb, and C. Cabassud, Evaluation of systems coupling vacuum membrane distillation and solar energy for seawater desalination, *Chem. Eng. J.*, **166**:596–606, 2011.

143. J. Blanco, S. Malato, P. Fernandez-Ibañez, D. Alarcon, W. Gernjak, and M. I. Maldonado, Review of feasible solar energy applications to water processes, *Renewable Sustainable Energy Rev.*, **13**:1437–1445, 2009.

144. Desertec Foundation, Red Paper: An Overview of the Desertec Concept, 2010. Retrieved July 15, 2011, from: http://www. desertec.org/fileadmin/downloads/desertec-foundation_redpaper_3rd-edition_english.pdf.

145. J. Blanco, D. Alarcon, G. Zaragoza, E. Guillen, P. Palenzuela, and M. Ibarra, Expanding CSP research frontier: Challenges to be addressed by combined solar power and desalination plants, in *Proc. of 16th Solar PACES Conf.*, Sept. 21–14, Perpignan, France, 2010.

146. C. Hoyer-Klick, The Union for the Mediterranean and the Mediterranean Solar Plan, in *Mediterranean Solar Plan Workshop*, Berlin, Germany, Oct. 28, 2008.

147. L. C. Spencer, A comprehensive review of small solar-powered heat engines: Part I. A history of solar-powered devices up to 1950, *Solar Energy*, **43**(4):191–196, 1989.

148. H. Price, E. Lüpfert, D. Kearney, E. Zarza, G. Cohen, R. Gee, and R. Mahoney, Advances in

parabolic trough solar power technology, *J. Sol. Energy Eng.*, **124**(2):109–126, 2002.

149. G. E. Cohen, D. W. Kearney, and H. W. Price, Performance history and future costs of parabolic trough solar electric systems, in *Proc. of 9th SolarPACES Intl. Symp., J. Phys. IV France*, **09**:169–179, 1999.
150. M. Geyer, A. Sevilla, J. A. Nebrera, and A. G. Zamora, Dispatchable solar electricity for summerly peak loads from the solar thermal projects Andasol-1 and Andasol-2, in *Proc. of 13th SolarPACES Conf.*, Seville, Spain, June 2006.
151. J. Schulte-Fischedisk, R. Tamme, and U. Herrmann, CDF analysis of the cool down behavior of molten salt thermal storage systems, in *Proc. of Energy Sustainability 2008*, Aug. 10–14, Jacksonville, FL, 2008.
152. G. Kronenberg and F. Lokiec, Low-temperature distillation processes in single- and dual-purpose plants, *Desalination*, **136**:189–197, 2001.
153. L. Yang and S. Shen, Assessment of energy requirement for water production at dual-purpose plants in China, *Desalination*, **205**:214–223, 2007.
154. I. Kamal, Integration of seawater desalination with power generation, *Desalination*, **180**:217–229, 2005.
155. N. Bouzayani, N. Galanis, and J. Orfi, Thermodynamic analysis of combined electric power generation and water desalination plants, *Appl. Thermal Eng.*, **29**:624–633, 2009.
156. F. Trieb, Concentrating solar power for seawater desalination, Aqua-CSP Study report, German Aerospace Center, Stuttgart, Germany, 2007. Retrieved July 15, 2011, from: http://www.dlr.de/tt/en/ desktopdefault.aspx/tabid-2885/4422_read-10813/.
157. R. Olwig, T. Hirch, and C. Sattler, Techno-economic analysis of combined concentrating solar power and desalination plant configurations in Israel and Jordan, in *Proc. of EuroMed 2010*, Oct. 3–7, Tel Aviv, Israel, 2010.
158. M. Moser, F. Trieb, and J. Kern, Combined water and electricity production on industrial scale in the MENA countries with concentrating solar power, in *Proc. of EuroMed 2010*, Oct. 3–7, Tel Aviv, Israel, 2010.
159. A. Ghobeity, C. J. Noone, C. N. Papanicolas, and A. Mitsos, Optimal time-invariant operation of a power and water cogeneration solar-thermal plant, *Solar Energy*, **85**(9):2295–2320, 2011.
160. C. Richter and J. Dersch, Methods for reducing cooling water consumption in solar thermal power plants, in *Proc. of 15th SolarPaces CSP Symp.*, Berlin, Germany, Sept. 15–18, 2009.
161. A. M. Blanco-Marigorta, M. V. Sanchez-Henriquez, and J. A. Pena-Quintana, Exergetic comparison of two different cooling technologies for the power cycle of a thermal power plant, *Energy*, **36**:1966–1972, 2011.
162. J. Blanco, D. Alarcon, P. Palenzuela, G. Zaragoza, C. Sattler, R. Olwig, K. Hennecke, R. El Navrawy, and B. Rashed, Assessment of CSP + D potential in the Mena Area, SolarPACES Task VI Report, Retrieved July 15, 2011, from: http://www.solarpaces.org/ Library/library.htm.
163. O. A. Hamed, H. A. Al-Washmi, and H. A. Al-Otaibi, Thermoeconomic analysis of a power/water cogeneration plant, *Energy*, **31**(14):2699–2709, 2006.
164. W. Short, D. J. Packey, and T. Holt, A manual for the economic evaluation of energy efficiency and renewable energy technologies. NREL/TP–462–5173, Golden, CO, 1995.

165. US Department of Energy, Concentrating Solar Power Commercial Application Study: Reducing Water Consumption of Concentrating Solar Power Electricity Generation, Washington, DC, 2009.

166. M. A. Green, K. Emery, Y. Hishikawa, and W. Warta, Solar cell efficiency tables (version 37), *Prog. Photovoltaics*, **19**:84–92, 2010.

167. S. R. Wenham, M. A. Green, M. E. Watt, and R. Corkish, *Applied Photovoltaics*, Earthscan, London, 2007.

168. E. Koutroulis, K. Kalaitzakis, and N. C. Voulgaris, Development of a microcontroller-based, photovoltaic maximum power point tracking control system, *IEEE Trans. Power Electron.*, **16**:46–54, 2001.

169. A. Ghermandi and R. Messalem, Solar-driven desalination with reverse osmosis: The state of the art, *Desalination Water Treatment*, **7**:285–296, 2009.

170. D. G. Harrison, G. E. Ho, and K. Mathew, Desalination using renewable energy in Australia, *Renewable Energy*, **8**:509–513, 1996.

171. A. Al Malki, M. Al Amri, and H. Al Jabri, Experimental study of using renewable energy in the rural areas of Oman, *Renewable Energy*, **14**:319–324, 1998.

172. B. S. Richards and A. I. Schäfer, Photovoltaic-powered desalination system for remote Australian communities, *Renewable Energy*, **28**:2013–2022, 2003.

173. S.-F. Cheah, *Photovoltaic Reverse Osmosis Desalination System*, ITN Energy Systems, Inc., Littleton, CO, 2004.

174. A. M. Thomson, *Reverse-Osmosis Desalination of Seawater Powered by Photovoltaics Without Batteries*, PhD Thesis, Loughborough University, Loughborough, UK, 2003.

175. B. S. Richards, D. P. S. Capão, and A. I. Schäfer, Renewable energy powered membrane technology. 2. The effect of energy fluctuations on performance of a photovoltaic hybrid membrane system, *Environ. Sci. Technol.*, **42**:4563–4569, 2008.

176. A. Joyce, D. Loureiro, C. Rodrigues, and S. Castro, Small reverse osmosis units using PV systems for water purification in rural places, *Desalination*, **137**:39–44, 2001.

177. A. M. Bilton, L. C. Kelley, and S. Dubowsky, Photovoltaic reverse osmosis—Feasibility and a pathway to develop technology, *Desalination Water Treatment*, **31**:24–34, 2011.

178. Dow, FILMTEC Membranes System Design: System Performance Projection, Dow Chemical Corporation, 2004.

179. M. Thomson and D. Infield, A photovoltaic-powered seawater reverse-osmosis system without batteries, *Desalination*, **153**:1–8, 2003.

180. S. A. Kalogirou, Seawater desalination using renewable energy sources, *Prog. Energy Combust. Sci.*, **31**:242–281, 2005.

181. E. Tzen, D. Theofilloyianakos, and Z. Kologios, Autonomous reverse osmosis units driven by RE sources experiences and lessons learned, *Desalination*, **221**:29–36, 2008.

182. I. de la Nuez Pestana, F. Javier García Latorre, C. Argudo Espinoza, and A. Gómez Gotor, Optimization of RO desalination systems powered by renewable energies, Part I: Wind energy, *Desalination*, **160**:293–299, 2004.

183. D. Herold and A. Neskakis, A small PV-driven reverse osmosis desalination plant on the island of Gran Canaria, *Desalination*, **137**:285–292, 2001.

184. E. S. Mohamed and G. Papadakis, Design, simulation and economic analysis of a stand-alone

reverse osmosis desalination unit powered by wind turbines and photovoltaics, *Desalination*, **164**:87–97, 2004.

185. E. Tzen, K. Perrakis, and P. Baltas, Design of a stand alone PV—Desalination system for rural areas, *Desalination*, **119**:327–333, 1998.
186. P. C. M. de Carvalho, R. S. T. Pontes, D. S. Oliveira, Jr., D. B. Riffel, R. G. V. de Oliveira, and S. B. Mesquita, Control method of a photovoltaic powered reverse osmosis plant without batteries based on maximum power point tracking, in *IEEE/PES Transmission and Distribution Conf. and Exposition: Latin America*, pp. 137–142, São Paulo, Brazil, Novem. 8–11, 2004.
187. A. Schies, J. Went, C. Heidtmann, M. Eisele, F. Kroemke, H. Schmoch, and M. Vetter, Operating control strategies and dimensioning of photovoltaic-powered reverse osmosis desalination plants without batteries, *Desalination Water Treatment*, **21**:131–137, 2010.
188. L. C. Kelley, *The Design and Control of a Thermal Management System for a Photovoltaic Reverse Osmosis System, Mechanical Engineering*, MS Thesis, Massachusetts Institute of Technology, Cambridge, MA, 2011.
189. Y. Effendi, Three years experiences for PVRO-desalination, in *Conf. Record of the Twentieth IEEE Photovoltaic Specialists Conf.*, vol. 2, pp. 1194–1199, Las Vegas, Nevada, Sep. 26–30, 1988.
190. K. E. Thomas, Overview of village scale, renewable energy powered desalination, National Renewable Energy Laboratory (NREL), Golden, CO, 1997.
191. Z. Al Suleimani and V. R. Nair, Desalination by solar-powered reverse osmosis in a remote area of the Sultanate of Oman, *Appl. Energy*, **65**:367–380, 2000.
192. P. C. M. de Carvalho, D. B. Riffel, C. Freire, and F. F. D. Montenegro, The Brazilian experience with a photovoltaic powered reverse osmosis plant, *Prog. Photovoltaics*, **12**:373–385, 2004.
193. M. A. Rayan, B. Djebedjian, and I. Khaled, Evaluation of the effectiveness and performance of desalination equipment in Egypt, in *8th Intl. Water Technology Conf.*, Alexandria-Egypt, March 26–28, 2004.
194. S. Abdallah, M. Abu-Hilal, and M. S. Mohsen, Performance of a photovoltaic powered reverse osmosis system under local climatic conditions, *Desalination*, **183**:95–104, 2005.
195. S. Bouguecha, B. Hamrouni, and M. Dhahbi, Small scale desalination pilots powered by renewable energy sources: Case studies, *Desalination*, **183**:151–165, 2005.
196. S. Dallas, N. Sumiyoshi, J. Kirk, K. Mathew, and N. Wilmot, Efficiency analysis of the SolarFlow—An innovative solar-powered desalination unit for treating brackish water, *Renewable Energy*, **34**:397–400, 2009.
197. D. B. Riffel and P. C. M. Carvalho, Small-scale photovoltaic-powered reverse osmosis plant without batteries: Design and simulation, *Desalination*, **247**:378–389, 2009.
198. D. Herold, V. Horstmann, A. Neskakis, J. Plettner-Marliani, G. Piernavieja, and R. Calero, Small scale photovoltaic desalination for rural water supply—Demonstration plant in Gran Canaria, *Renewable Energy*, **14**:293–298, 1998.
199. E. Tzen, D. Theofilloyianakos, M. Sigalas, and K. Karamanis, Design and development of a hybrid autonomous system for seawater desalination, *Desalination*, **166**:267–274, 2004.
200. E. S. Mohamed, G. Papadakis, E. Mathioulakis, and V. Belessiotis, A direct coupled photovoltaic seawater reverse osmosis desalination system toward battery based systems—

A technical and economical experimental comparative study, *Desalination*, **221**:17–22, 2008.

201. SpectraWatermakers, SSW 3500 Datasheet. Retrieved Feb. 5, 2009, from http://www. spectrawatermakers.com/landbased/products_ssw3500.php.
202. H. M. N. Al Madani, Water desalination by solar powered electrodialysis process, *Renewable Energy*, **28**:1915–1924, 2003.
203. J. M. Ortiz, E. Expósito, F. Gallud, V. García-García, V. Montiel, and A. Aldaz, Desalination of underground brackish waters using an electrodialysis system powered directly by photovoltaic energy, *Solar Energy Mater. Solar Cells*, **92**:1677–1688, 2008.
204. N. Ishimaru, Solar photovoltaic desalination of brackish water in remote areas by electrodialysis, *Desalination*, **98**:485–493, 1994.
205. M. R. Adiga, S. K. Adhikary, P. K. Narayanan, W. P. Harkare, S. D. Gomkale, and K. P. Govindan, Performance analysis of photovoltaic electrodialysis desalination plant at Tanote in Thar desert, *Desalination*, **67**:59–66, 1987.
206. O. Kuroda, S. Takahashi, K. Wakamatsu, S. Itoh, S. Kubota, K. Kikuchi, Y. Eguchi, Y. Ikenaga, N. Sohma, and K. Nishinoiri, An electrodialysis sea water desalination system powered by photovoltaic cells, *Desalination*, **65**:161–169, 1987.
207. L. L. Kazmerski, Photovoltaics: A review of cell and module technologies, *Renewable Sustainable Energy Rev.*, **1**:71–170, 1997.